ScientificScholar®
Knowledge is power
Publisher of Scientific Journals

https://arabjchem.org

Arabian Journal of Chemistry

2025 18 (3) 1272024

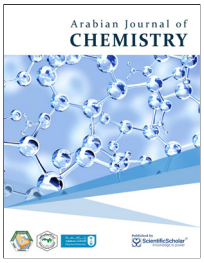

Review Article

Hollow sphere TiO_2: Synthesis and its application for dye-sensitized solar cells

Khusna Arif Rakhman[a], Nurul Hidayat Aprilita[b], Rohana Adnan[c], Indriana Kartini[b,*]

[a]Department of Chemistry Education, Universitas Khairun, Ternate, Indonesia
[b]Department of Chemistry, Universitas Gadjah Mada, Yogyakarta, Indonesia
[c]School of Chemical Sciences, Universiti Sains Malaysia, 11800 Gelugor, Penang Malaysia

ARTICLE INFO

Keywords:
DSSC
Hollow sphere TiO_2
Photovoltaic
Solar cells
TiO_2

ABSTRACT

The architecture of semiconductor oxides as the core photoanodes in the dye-sensitized solar cells affecting the energy conversion of the dye-sensitized solar cells (DSSC) has been a slightly neglected parameter. Herein, we study that the morphology of hollow sphere (HS) TiO_2 as the semiconductor photoanode of DSSC has proven to result in the power conversion efficiency (PCE) higher than the solid sphere of TiO_2, and other morphology such as nanotube, nanowire, and nanorod. Affecting the photocurrent density (Jsc) and PCE, efficient electron transfer was achieved in HS TiO_2. The percentage of PCE of DSSC using HS TiO_2 semiconductor is also influenced by physical properties such as particle size and shell thickness, which influence the dye-loading capacity, the rate of electron transfer, and the scattering effects in visible light harvesting. This review discusses the synthesis and characterization of HS TiO_2 from two different synthesis pathways, the one-pot and two-step synthesis, and the modification of HS TiO_2 to improve the efficiency of DSSC.

1. Introduction

The development of renewable energy remains as a great challenge in overcoming the depletion of fossil energy and its negative impact on the environment. Dye-sensitized solar cell (DSSC) is one of the renewable energy devices receiving great attention because it can directly convert sunlight into electrical energy [1]. DSSC is a light and flexible solar cell with simple, low-cost fabrication and can be designed for green devices [2–4]. The main components of DSSC are: a thin layer of semiconductor mesopore, dye molecules as sensitizers, electrolytes, and counter electrodes, which are attached to a conducting glass substrate [4]. A thin layer consists of transparent glass or flexible plastic substrate that can transmit solar radiation into the photoanode. The glass substrate provides a surface for the deposition of semiconductor metal oxides (photoanode) and catalyst material (counter electrode). The photoanode has good electrical conductivity properties to collect the current from the dye-sensitized TiO_2 layer and transfer it to the external circuit [5]. Mesoporous photoanodes are metal oxide semiconductors that play an important role in the loading of dyes and the transfer of electrons to the external circuit [6]. Dye sensitizer (photosensitizer) is a special component in DSSC and is the essence of this type of solar cell. The photosensitizer is attached to the semiconductor through covalent bonds and is responsible for harvesting sunlight, especially in the visible region [7]. Electrolytes are a redox salt solution (e.g. I/I_3^-), which is injected between a thin layer of photoanode and the calculating electrode and functions to regenerate the oxidized dye. The last component is the counter electrode (CE), which consists of a thin layer of deposited catalyst. The arrangement of energy levels in all DSSC components must be in harmony to facilitate the transfer of electrons in converting light to electrical energy. Sequentially, the arrangement of energy levels starts from the lowest energy level of the lowest unoccupied molecular orbital (LUMO) of the dye, followed by the conduction band (CB) of the photoanode semiconductor, then the redox potential of the electrolyte, and the energy level of the highest occupied molecular orbital (HOMO) level of the dye [6].

The efficiency of DSSC is influenced by several parameters such as photocurrent (*Jsc*), photovoltage (*Voc*), and fill factor (FF) [8–10]. Meanwhile, *Jsc* relies on the efficiency of light harvesting, injection, and electron collection efficiency [11–13]. According to Ahmad *et al.* [14], limiting the recombination rate can increase the electron density in the conduction band of the semiconductor as well as increases the quasi-Fermi energy level, and *Voc*. All of these parameters are closely related to the electron transfer mechanism in the DSSC component. Capturing electrons in a semiconductor is the beginning of photovoltage and the flow of electrons to produce photocurrent [15]. The transfer of electrons in the DSSC component starts from the absorption of photons (hv) by the photosensitizer (dye), which then causes the electron from the dye molecule (D) to experience excitation from the HOMO to the LUMO energy level, as shown in the Eq. (1) [5]:

$$D_{adsorbed} + h\nu \rightarrow D^*_{adsorbed} \quad (1)$$

The excited dye molecule then injects electrons into the conduction band (CB) of the semiconductor, leaving the dye molecule oxidized (D^+) (Eq. 2):

$$D^*_{(adsorbed)} \rightarrow D^+_{(adsorbed)} + e^-_{(injected)} \quad (2)$$

The injected electrons are then transmitted through the semiconductor, followed by the transfer of electrical energy through a conductive substrate, external circuit, and a counter electrode (CE, Eq. 3):

*Corresponding author:
E-mail address: indriana@ugm.ac.id (I. Kartini)

Received: 31 October, 2024 **Accepted:** 18 February, 2025 **Epub Ahead of Print:** *** **Published:** 17 April 2025
DOI: 10.25259/AJC_127_2024

$$e^-_{(injected)} + CE \rightarrow e^-_{(CE)} + \text{electrical energy} \quad (3)$$

Transport of electrons through diffusion process is strongly influenced by the intensity of the incident light, electron concentration, and the efficiency of media transport [5]. At the counter electrode, electrons in the electrolyte component are reduce from I_3^- to I^-. At the same time, the oxidized dye (D^+) returns to the ground state (D) after receiving electrons from I^- and thus completing the regenerative cycle (Eqs. 4 and 5).

$$I_3^- + 2.\ e^-_{(CE)} \rightarrow 3I^-_{(CE)} \quad (4)$$

$$D^+_{(adsorbed)} + 3/2I^- \rightarrow D_{(adsorbed)} + 1/2I_3^- \quad (5)$$

However, in its application, not all electrons can be transferred perfectly in a DSSC device. Electron recombination always accompanies the electron diffusion process in this device. Three types of recombination co-occur with the electron transport process [5,16]. The first is direct recombination; it describes the lifetime of the excited state of the dye molecule. In other words, due to the absorption of sunlight, the excited electrons in the conduction band (CB) return directly to the ground state in the dye molecule's valence band (VB) (Eq. 6):

$$D^+_{(adsorbed)} + e^-_{(injected)} \rightarrow D_{(adsorbed)} \quad (6)$$

Second, recombination in the injection of electrons in the semiconductor (SC) with oxidized dye (Eq. 7):

$$D^+_{(adsorbed)} + e^-_{(SC)} \rightarrow D_{(adsorbed)} \quad (7)$$

The third is the recombination of injected electrons in the surface of the semiconductor (SC) with the acceptor in the electrolyte (Eq. 8).

$$I_3^- + 2.\ e^-_{(SC)} \rightarrow 3I^-_{(anode)} \quad (8)$$

Both reactions in Eqs. (7) and (8) are undesirable as they may result in the losses in the cell efficiency.

Two of the three factors that affect electron transport in the DSSC mentioned above are dye concentration and the efficiency of the electron transport medium [5]. The high dye concentration allows the release of large amounts of electrons from the dye. The efficiency of the electron transport medium is related to the storage capacity and the speed of transferring electrons from the conduction band of the dye molecule to the conduction band of the TiO_2 semiconductor and subsequently to the external circuit [17]. In DSSC, metal oxide semiconductors are photoelectrodes that play a role in electron collection (or electron capture) and transfer, such that their physical properties and structure determine the performance of the DSSC [18]. The structure and physical properties of semiconductors, such as surface area, morphology, and band gap, are some of the factors that affect the efficiency of DSSC [19]. In principle, the efficiency of DSSC depends on the dye loading concentration, and the electron transport speed of the component is strongly influenced by the surface area and pore size of the semiconductor. Whereas the surface area and pore size of the semiconductor are related to the particle size and morphology of the material [20–22].

Various modifications of the semiconductors have been conducted to enhance the efficiency of DSSC. For instance, Ma *et al.* [23] reported an enhancement in electron transport from the TiO_2 double-layer formation. The decrease in particle size results in a blue shift in the band gap of the TiO_2 semiconductor. It has an impact on the arrangement of energy levels and electron transfer rates in the device, and the smallest particle size results in the best DSSC efficiency [24]. Examples of the modifications reported in the literature include coating of semiconductor surface with TiO_x or $TiCl_4$ solution to reduce the excessive recombination rate [3], incorporating plasmon material as a composite to accelerate electron transfer [25], and modifying the surface morphology in order to increase the surface area to increase the dye loading [26] and their electric properties [22]. A semiconductor with a high specific surface area has a high adsorption capacity. Meanwhile, a large pore volume benefits the electrolyte injection and effective contact between the electrolyte and the photoanode, thereby increasing the photoelectric conversion performance of DSSC [1].

TiO_2 nanoparticles with high specific surface area and sufficient dye adsorption capacity are needed to increase the light-harvesting efficiency (LHE) [27]. TiO_2 with specific morphology can increase the scattering effect of incident light [26]. TiO_2 is a suitable material for use in photoanode applications [17] compared to other metal oxides (such as ZnO, Nb_2O_5, SnO_2, and WO_3) because it achieves the highest energy efficiency [6]. TiO_2 has wide bandgap, non-toxic, is stable, ecologically benign, cost-effective, and has long-term stability against photo corrosion and chemical corrosion [28–31]. In recent years, research on the morphology of TiO_2 as a semiconductor in DSSC reported that hollow sphere HS TiO_2 was the best at increasing PCE compared to several other forms, such as nanorods, nanoflowers, and nanotubes. The spherical geometry of these hollow structures facilitates Mie scattering, effectively trapping incident light within the photoanode and prolonging the optical path length. This increased light interaction boosts photon absorption by the dye molecules, thereby enhancing the photocatalytic performance of the DSSC [32]. Moreover, the hollow nature of HS TiO_2 provides a high surface area, offering abundant sites for dye loading [33–36].On the other hand, the hollow structures exhibit good light trapping, charge separation and transport, and surface reactions in photocatalytic applications [37–39]. The improved efficiency in light trapping is attributed to the multiple directions of light scattering and the large surface area photon-retarding effect. Additionally, the hollow structure suppresses the recombination of e^- and h^+, promoting photocatalytic activity by reducing the charge recombination rate [40], thereby enhancing the light-trapping effect in the photocatalytic process [41]. HS TiO_2 with a high specific surface area and sufficient dye adsorption capacity has the potential to enhance electron transfer rates, LHE, and scattering effects to improve DSSC efficiency.

Fabrication of HS TiO_2 for the development of DSSC has shown promising advancements in efficiency, as reported by various authors [5,28]. For instance, Tamilselvan and Shanmugan [42] reported an efficiency of 11% using bio-nano materials. Key areas of improvement include molecular engineering or synthesis methods, carrier transport materials, efficient sensitizers, and better electrodes [43,44]. Hydrothermal/solvothermal and sol-gel methods have been widely used to prepare HS TiO_2 with various morphology and specific surface area. Exploring efficient HS TiO_2 fabricating methods to obtain products with uniform sizes and stable hollow structures is a lengthy process. Until now, there has been a lack of review covering TiO_2 HS specifically for DSSC applications. Therefore, the present review discusses the HS TiO_2 architecture and explores the synthesis methods, photovoltaic characteristics, and modifications made to improve the efficiency of DSSC. Obtaining precise and significant information about the synthesis pathway and characteristics of HS TiO_2 for photoanode applications is the relevant objective of this review.

2. Morphology Effect

A good photoanode is described by a high surface area and light scattering [45,46]. The development of DSSC using commercial TiO_2 improves surface area; however, it does not enhance light scattering because the particle diameter is smaller than the wavelength of incident light. Previously, mesoporous multilayer DSSC photoanodes with high surface area and high light scattering capability with an incident photon conversion efficiency of 10% have been developed [47]. Mesoporous materials with pore diameters ranging from 2 to 50 nm possess a continuous network of interconnections, leading to a high surface area and light scattering. Due to these advantages, mesoporous materials serve as a standard for the development of DSSC [48]. However, the mesoporous structure often exhibits low conductivity, which can facilitate the recombination of electrons. Consequently, new nanostructures with high conductivity and enhanced dye loading have become the focus of the next generation of photoanodes [47]. To fulfill the two basic requirements of a good photoanode—high dye loading and light scattering capabilities—the development of TiO_2 based photoanodes is still ongoing research. Table 1 compares the different TiO_2 morphologies that have been developed for photoanodes with dye loading using commercial dye N719 at the concentration of 5×10^{-4} M and its photovoltaic parameters.

Anatase phase TiO_2 nanoparticles with a wide band gap are the most effective materials for photoanodes due to their cost efficiency, good stability, easy availability, and compatible optical and electronic properties [22]. TiO_2 with different morphologies, such as nanotubes, urchin-like, and hollow nanoparticles exhibiting different PCEs, have

Table 1. Summary of the performance of different TiO_2 nanostructure morphologies for DSSC photoanode reported in the literature.

Morphology	*Jsc* (mA cm^{-2})	*Voc* (mV)	FF (%)	PCE (%)	References
Urchin-like	12.72	71.60	67.03	6.10	[35]
Nanowire	3.60	86.80	67.60	2.12	[49]
Nanotubes	10.48	83.50	68.12	5.96	[49]
Nanotubes array	10.15	74.50	62.00	4.69	[33]
Nanorods	8.88	66.00	47.00	2.75	[34]
Hollow nanoparticles	15.80	74.00	71.00	8.30	[36]
Nanoparticles	4.30	69.00	72.00	2.14	[50]
Nanoflower	5.10	79.70	72.60	2.95	[51]

Jsc: short circuit current density, *Voc*: open circuit voltage, FF: Fill factor, PCE: Power conversion efficiency

been reported (Table 1). It can be seen that nanotubes, urchin-like, and hollow nanoparticles (HNPs) produce high PCE, above 5.0%. The different morphology of TiO_2 changes the pore characteristics and the surface area of the material, which also affects the *Jsc* value. A smaller TiO_2 solid particle size can provide a larger surface area to improve the amount of loading of dyes and their *Jsc* [24,28]. For example, the use of nanotubes (NTs) TiO_2 with a surface area of 64.22 m^2 g^{-1} and pore size of 3-10 nm produced dye loading of 103.1 nmol cm^{-2}, *Jsc* of 10.48 mA cm^{-2}, and PCE of 5.96% [46]. In another study, the urchin-like TiO_2 (ULT) that has a higher pore size distribution of 3-60 nm resulted in a higher *Jsc* of 12.72 mA cm^{-2} and optimal dye adsorption capacity of about 319.73 nmol cm^{-2} and PCE of 6.10% [35]. The hollow sphere has been reported to produce the highest PCE than other morphologies; photovoltaic with a *Jsc* value of 15.8 mA cm^{-2} and PCE of 8.3% has been produced from HNPs with a surface area of 129 m^2 g^{-1} and particle diameter ~100 nm [36]. The unique structural properties of HNPs allow for enhanced light-harvesting capabilities and reduced electron recombination, which are critical for improving overall efficiency in DSSCs. As a specific type of HNPs, HS TiO_2 represents an evolution in design that retains these benefits while potentially addressing any limitations in conductivity or charge transport. Therefore, HS TiO_2 is positioned as a promising candidate for further development as a semiconductor in DSSCs, leveraging its excellent properties to maximize efficiency and performance in solar energy applications.

The *Jsc* depends on the light-harvesting efficiency, injection, and electron collection efficiency mentioned in the early section. Recent studies have demonstrated significant improvements in DSSC performance using hierarchical TiO_2 structures. Hierarchical nanostructures are integrated architectures comprising well-ordered nanoscale subunits with zero, one, two, or three-dimensional architectures [52], including nanostructures such as quantum dots, nanofibers, nanorods, nanowires, nanosheets, nanoflowers, nanospheres, or a combination of these architectures [53]. These structures combine the advantages of nanoparticles and larger spheres or rods, offering enhanced dye loading, light scattering, and electron transport [54]. It is reinforced by a hollow structure to improve the surface scattering of light and enhance the incidence of harvesting light [55]. A detailed discussion of the photovoltaic characteristics of hollow spheres TiO_2 has been presented in Section 3.

3. Synthesis of HS TiO_2

Generally, HS TiO_2 can be produced by two synthesis methods: hydrothermal/solvothermal and sol-gel (Figure 1). The hydrothermal/solvothermal method has a single-step synthesis. Meanwhile, the sol-gel method was a two-stage synthesis (Table 2). Synthesis of HS TiO_2 with several methods and templates can produce different particle sizes. Hydrothermal/solvothermal methods produce HS TiO_2 more than 100 nm in diameter [56], the largest among other methods. The sol-gel (carbon-based) template (SGCT) method produced more than a 50 nm diameter. Meanwhile, HS TiO_2, which is produced using a sol-gel hard template (SGHT) method, one of which uses SiO_2, can produce a diameter of more than 25 nm [57]. Based on the findings from the previous studies Table 2 presents the diameters of the HS TiO_2 produced by the SGHT > SGCT > hydrothermal/solvothermal method.

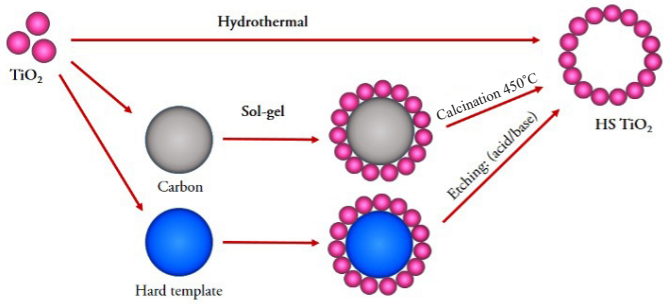

Figure 1. Schematic of synthesis of HS TiO_2.

3.1. Hydrothermal/solvothermal method

Hydrothermal/solvothermal methods were used in many nanoparticle fabrications in the ceramic industry using an aqueous or nonaqueous solution in an autoclave at a high temperature and pressure [58]. In this condition, supercritical fluids are formed and significantly improve the solubility of solid precursors resulting in the formation of nanostructures. In particular, wet fabrication by hydrothermal/solvothermal methods utilizing physical phenomena such as the Kirkendall effect and Ostwald ripening has been widely used to produce hollow nanostructures [59,60].

3.1.1. Kirkendall effect

Synthesis of HS TiO_2 by the solvothermal method using ethanol as the solvent at 180°C for 24 hrs resulted in the 1 μm-anatase phase material with a pore size of 5.2 nm and surface area of 242 m^2 g^{-1}. Hydrothermal synthesis of HS TiO_2 can take place *via* two formation mechanisms: the Kirkendall effect or Ostwald ripening [61]. Chen *et al.* [62] reported the production of a pure anatase phase of HS TiO_2 with 300–400 nm in diameters and a wall thickness of approximately 50 nm, using polyethyleneimine (PEI), which acts as a stabilizing and templating agent *via* solvothermal method. Time-dependent morphological evolution using transmission electron microscopy (TEM) analysis confirmed the formation of HS TiO_2 *via* the Kirkendall effect (Figure 2). In the synthesis of HS TiO_2 through the Kirkendall effect, solid nanospheres are formed at the beginning of the reaction (Figure 2a) (before heating). After heating at 180°C for 6 hrs, the nanosphere size and surface roughness increased, and a small cavity began to form (Figure 2b). When the reaction time increased to 16 hrs, the increase in the nanosphere particle size and inner cavity size was observed (Figure 2c). Meanwhile, different quantity of PEI was associated with the different viscosity of the reaction system and the adsorption of PEI molecules on the TiO_2 surface and these controlled the morphology of the TiO_2 produced [62]. Chen *et al.* [62] and Zhu *et al.* [63] reported that calcination treatment after the completion of the reaction at 400 to 700°C further enhanced the crystallinity of the TiO_2 without changing the crystalline phase.

The Kirkendall effect basically refers to the process of nonequilibrium mutual diffusion through the atoms in a diffusion couple. This causes supersaturation of the vacancies at the interface, and further condensation of the excess vacancies and interdiffusion leads to the formation of a hollow sphere [64,65]. The Kirkendall effect has been used in the fabrication route to form HS. However, not every particle size, shell thickness, or material crystallinity can be obtained from this route [66]. Basically, synthesis through the Kirkendall effect requires a surfactant to produce HS TiO_2. The Kirkendall effect is a one-pot synthesis with a two-step process that can produce HS TiO_2. The first stage is the formation of vacancies in the TiO_2 nanostructure. In this stage, the faster-diffusing species will be confined into a nanocrystal core. The vacancy-injection net rate increased, as evidenced by the high surface-to-volume ratio of the transformed particles and the absence of defects in the TiO_2 nanostructure. In the next stage, supersaturated void clouds will gather together and form a cavity of HS TiO_2 (Figure 2d) [67].

Table 2. Synthesis of HS TiO_2.

Method	Materials		Synthesis condition		Characteristics				References
	Template/surfactant	Precursor	Temperature (°C)	Time (hour)	Surface area (m^2/g)	Particle size (nm)	Pore size (nm)	Wall thickness (nm)	
Hydrothermal/ solvothermal	Urea, tert-Butyl ammonium hydroxide	Titanium isopropoxide	180	24	78.3	3000			[68]
	Tween 60 & polyethylene glycol	Titanium isopropoxide	180	24	155	1000			[69]
	Oxalic acid	Titanium n-butoxide	180	10		450		30	[70]
	Polyethyleneimine	Tetrabutyl titanate	180	24		100-200	2-50		[63]
	Glucose, polyvinyl pyrrolidone (PVP)	Titanium tetrabutoxide (TBOT)	125	72		75-100		10-14	[71]
	Valeric acid, butyric acid	Titanium isopropoxide	190	18	83	514	7		[72]
	NH_4F, $CO(NH_2)_2$	$Ti(SO_4)_2$ & $Zn(NO_3)_2 \cdot 6H_2O$	180	6	55.985	~2000			[73]
	Octanoic acid	Titanium isopropoxide	190	18	47.5, 52.1, 55.9, 54.0	220, 440, 620, 800			[55]
	Polyethyleneimine (PEI)	Butyl titanate	180	24		300-400		50	[62]
	Tween 20	Titanium isopropoxide	180	24	242		52		[74]
	Acetylacetone	Tetrabutyl titanate	200	10		900	~700	~90	[75]
	Urea	Ti plate: $TiCl_4$:H_2SO_4	200	12		1000		20-30	[76]
		Titanium(IV) butoxide (TBT)	220	5		1000-2000			[56]
		Tetrabutyl titanate	130	48		10		2-4	[67]
	Oxalic acid	Tetrabutyl titanate	180	6	166.2	1000-1500	3-33	150	[77]
	PVP, NaF	Tetrabutyl titanate	110	2, 3, 4, 5		320			[78]
	H_3BO_3	AHFT: $(NH_4)_2TiF_6$	90	0.25	102	800-1000			[79]
		Titanium (IV) chloride	220	6	50.2	1000	18.7		[80]
		Tetrabutyl titanate (TBOT)	220	5		1200		100	[81]
Sol-gel (carbon-based template)	Polystyrene	TTIP	50	1.5		~380, ~190		~60, ~50, ~100	[82]
	Polystyrene	Tetra-n-butyl titanate (TBT)	RT	0.5	41, 36, 34		17, 21, 18		[83]
	Polystyrene	Titanium tetrabutoxide (TBOT)	80	2		147, 151, 155, 159		9, 14, 17, 23	[84]
	Polystyrene	TBOT	70	2	96.7, 54.2	332, 412	11.3, 8.1	28, 50	[85]
	Polystyrene	Titanium ethoxide	70	12		60-365		100, 110, 120, 130	[86]
	Poly styrenemethacrylic acid (PSA)	$Ti(SO_4)_2$	50	1.5	20.821, 52.412, 113.335	1000-120			[87]
	Carbon hollow sphere	Titanium(IV) n-butoxide ($Ti(OBu)_4$)	24.85	24			400-600	20-60	[88]
	Glucose	Titanium tetraisopropoxide (TTIP)		1		250-350			[89]
	Polystyrene	tetrabutyl titanate (TBT), tetrabutylzirconate (TBZ) (1:1)	25	3		190			[84]
	Polystyrene	tetrabutyl titanate (TBT)	80	6	58.3	300		13.3	[90]
	CTAB	$TiCl_4$, $(CH_3CH_3CHO)_4Ti$		2		94.9	36000		[57]
	Polydopamine (PDA)	Tetrabutyl titanate (TBT)	RT	2		568		105	[91]
	Anhydrous dextrose	Titanium (IV) butoxide	RT	1	138.07, 101.98, 54.53	667.98, 327.03, 170.91		46.98, 28.36, 32.62	[92]
	Polystyrene	Tetrabutyl titanate (TBT)	RT	20		85	59	16	[93]
Sol-gel (hard template)	SiO_2: (TEOS)	Titanium tetraisopropoxide (TTIP)	55, 50, 40, 35, 20	6		25, 50, 75, 100, 125			[94]
	SiO_2: (TEOS)	Titanium tetraisopropoxide (TTIP)				50			[95]
	SiO_2: (TEOS)	Titanium tetraisopropoxide (TTIP)	5	6		25, 50, 100		5.5, 11, 20.5	[96]
	SiO_2: (TEOS)	Titanium n-butoxide (TBOT)	85	2		360		Outer: 30, Inner: 35	[97]
	SiO_2: (TEOS)	Titanium tetraisopropoxide (TTIP)	4	6	246	120			[98]
	Au: $HAuCl_4$	TiF_4	100	1		200		60	[99]
	SiO_2: (TEOS)	Titanium tetraisopropoxide (TTIP)	4	6	129	~100	Cav: 5, Intra: 35		[36]
	$K_3PW_{12}O_{40}$	$Ti(SO_4)_2$	125	8		500-1000			[100]
	$CaCO_3$	TEOS, TBOT	RT	3	113			<181	[101]
	Au: $HAuCl_4$	TiF_4	180	1		~200			[102]
	SiO_2: (TEOS)	tetrabutyl titanate (TBT)	85	1.7		~200		~50	[103]
	SiO_2: (TEOS)	Titanium tetraisopropoxide (TTIP)		12		140		20	[104]
	SiO_2: (TEOS)	Titanium n-butoxide (TBOT)		2		185		30	[105]
	SiO_2: (TEOS)	Titanium n-butoxide (TBOT)	RT	2		455, 470, 494, 530, 606		23, 31, 41, 61, 99	[106]
	SiO_2: (TEOS)	Titanium Isopropanol	25	1.5	74.3	204		17	[107]
	SiO_2: (TEOS)	Titanium n-butoxide (TBOT)	45	24		480		20-30	[108]

RT: Room temperature, PVP: Polyvinylpyrolidone, NaF: Sodium flouride, TTIP: Titanium isopropoxide, CTAB: Cetyltrimethylammonium Bromide

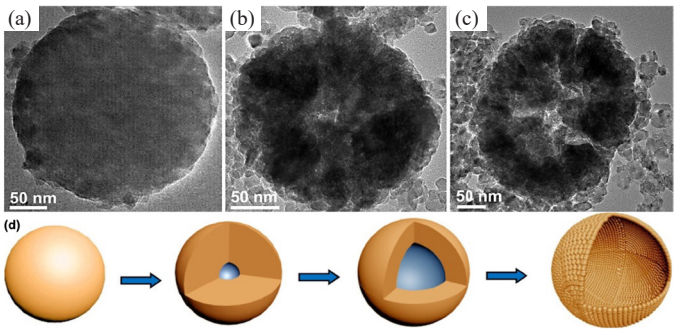

Figure 2. TEM images (a-c): the formation of hollow TiO_2 at different reaction times of 0, 6, and 16 h. (d) Scheme illustration of the formation of a TiO_2 hollow nanosphere *via* the Kirkendall effect [62]. Licensed by Elsevier.

3.1.2. Ostwald ripening

The formation of HS TiO_2 through Ostwald ripening is a one-pot synthesis without a template, surfactant, and calcination process. This process is a growth from a solid bulk structure, spherical solid structure to a spherical hollow structure [90]. High pressure can affect colloidal crystallite suspensions, causing compression and potentially altering electrostatic properties while also increasing orientational order and crystallite growth [109]. Ostwald ripening is also described as dissolving the core and recrystallizing the shell, resulting in a cavity of the structure (Figure 3) [70].

The production of HS TiO_2 through Ostwald ripening begins with the etherification of alcohol as a solvent by H_2O. The TiO_2 precursor undergoes hydrolysis and forms a cavity in the hollow structure (Figure 4). Synthesis with this principle is very dependent on the reaction temperature. At temperatures less than 140°C, alcohol etherification is difficult, and hydrolysis of TiO_2 precursors cannot be carried out, so HS TiO_2 is not formed. When the temperature exceeds 140°C, the system allows for the formation of HS TiO_2 from the precursor, but the reaction rate will vary at different temperatures [90]. In a reaction rate investigation, Nguyen and Kim [110] reported that HS TiO_2 was successfully produced through Ostwald ripening at 220°C. HS TiO_2 with anatase crystal phase was formed after the reaction was running for 5 h, and the crystallinity and structure after being extended 7 hrs did not change. Meanwhile, control of the diameter of HS TiO_2 can be done by adjusting the addition of Ti precursors, but this can impact decreasing the pore diameter and surface area [56]. Excess precursors are also thought to reduce the core's dissolution process in cavity formation.

3.2. Sol-gel method

3.2.1. Sol-gel carbon-based template

Fabrication of HS TiO_2 by the sol-gel method has a two-step synthesis. Templating the HS TiO_2 by producing a core@shell structure is the first step, and removing the templates (core) to produce a hollow sphere is the second step. The sol-gel method uses two templates to get core@shell, carbon-based, and hard templates. Polydopamine (PDA) has also shown good performance as a carbon-based template (CBT) in the manufacture of HS TiO_2. The synthesis of HS TiO_2 with a PDA template was reported by Ma *et al.* [91], resulting in HS TiO_2 with a diameter of ~500 nm for photocatalytic applications.

In principle, PDAs have demonstrated the ability to effectively adhere to many surface materials such as metals, oxides, ceramics, polymers, carbon nanotubes, and magnetite nanoparticles [111]. The other CBT used to produce HS TiO_2 from the sol-gel process include poly(styrenemethacrylic acid) (PSA) [87], glucose [89], and polystyrene (PS) [83]. As a template, PS is produced by the polymerization of styrene. To be able to deposit TiO_2 on the PS surface, it is necessary to add a cationic initiator such as 2-(methacryloyloxy) ehyl trimethylammonium chloride (DMC) (Figure 5) [112]. Similarly, cationic polymerization initiators like 2,2-azobis-(isobutyramidine) dihydrochloride (AIBA) [85] and potassium persulfate (KPS) [84] have been reported to provide positive charges on the surface of PS and assist the formation of PS@TiO_2 (Figure 5). The formation of HS

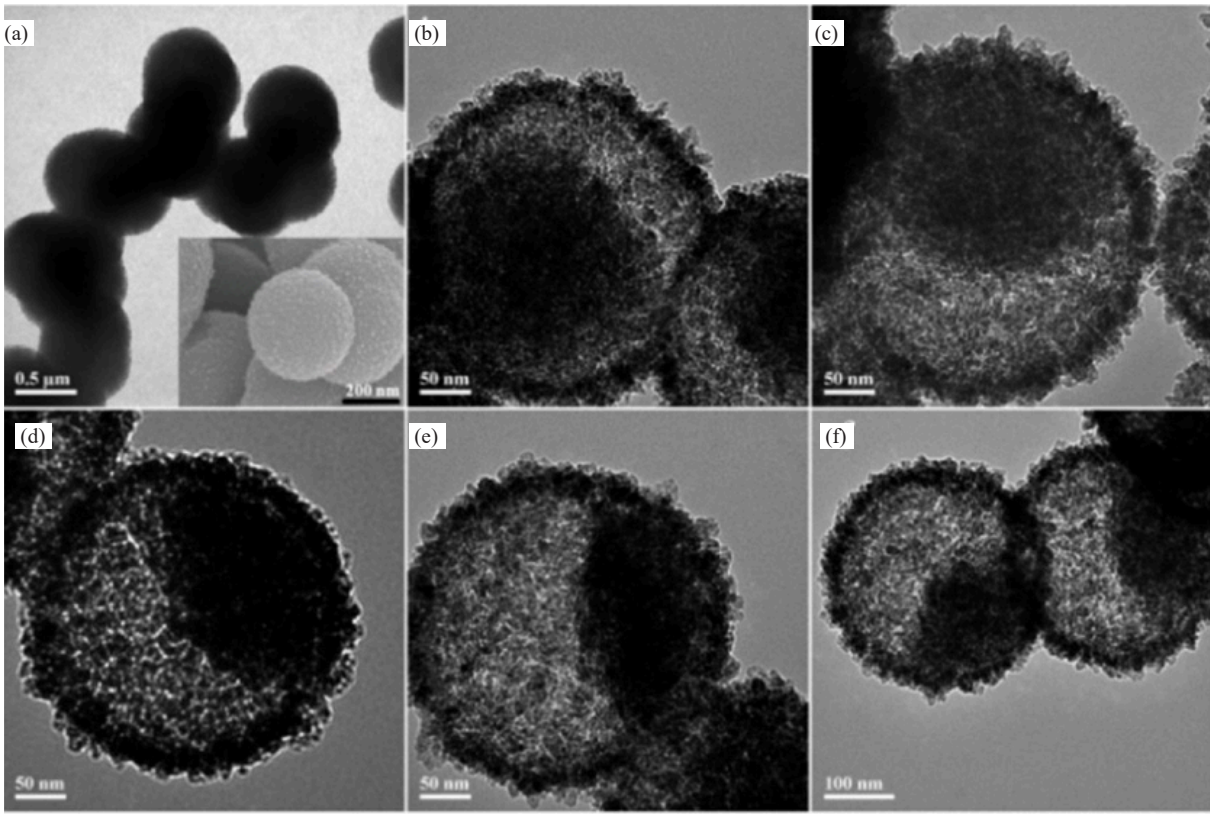

Figure 3. TEM images of the samples with different reaction times: (a) 3 h at 150°C. If not stated, all the reactions are at 180°C. (b) 2 h; (c) 3 h; (d) 4 h; (e) 5 h; (f) 6 h; [70]. Licensed by American Chemical Society. TEM: Transmission electron microscopy.

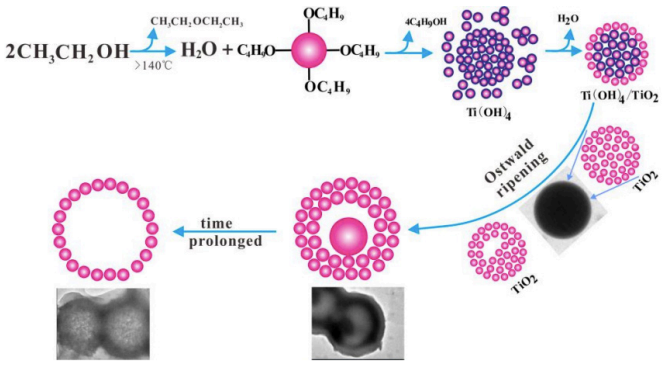

Figure 4. Scheme to illustrate the formation process for hollow TiO_2 spheres [90]. Licensed by Elsevier.

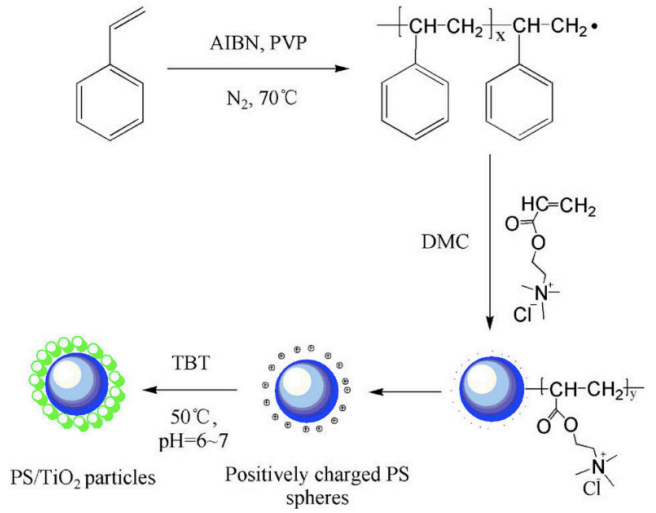

Figure 5. Synthetic route of PS/TiO_2 core@shell particles [112]. Licensed by Elsevier.

TiO_2 with different particle sizes can be affected by pH and the ratio of the addition of titania precursor to solvent. For example, Kanjana *et al.* [92] reported that a reaction at low pH (acidic) resulted in larger particle size compared to reactions conducted under neutral or alkaline conditions. In addition to that, Syoufian *et al.* [84] reported that adding an excessive amount of precursor increased the particle size of HS TiO_2. The TiO_2 template removal to produce the hollow structure can be carried out simultaneously with calcination. Synthesis with this method can also produce HS TiO_2 at low pressures to yield particle sizes of hundreds to thousands of nm and shell thicknesses of up to hundreds of nm (Table 2).

3.2.2. Sol-gel hard template

The sol-gel hard template method is a two-step process commonly used to synthesize hollow nanostructures like HS TiO_2 [113]. The first stage is templating core@shell with SiO_2 as the core coated with TiO_2 in the shell. The second stage is the formation of HS TiO_2 by removing the core from the core@shell (Figure 6). The synthesis of HS TiO_2 through the formation of SiO_2@TiO_2 was carried out at alkaline pH to prepare a SiO_2 template with a negative surface charge (-) to interact with the titania precursor prepared in acidic medium (positive surface charge). The synthesis of HS TiO_2 can be conducted by SiO_2 core from SiO_2@TiO_2 material using ammonia or sodium hydroxide solution by etching [95–97, 107]. The fabrication process involves the introduction of ammonium ions (NH_4^+), which bind to the negatively charged SiO_2 surface through electrostatic interactions with the –OH groups, creating a positively charged surface. This step ensures strong adhesion of the titania precursor to the SiO_2 template, enabling the formation of a uniform TiO_2 shell.

The accumulation of NH_4^+ on the surface of SiO_2 encourages interaction with the negatively charged –TiOH group and, through a condensation process with an NH_4^+ catalyst forms SiO_2@TiO_2. The formation of a hollow material can be determined by core@shell (CS) as the initial product of HS TiO_2 synthesis. In manufacturing the SiO_2@TiO_2, SiO_2 is widely used as a core because it is easy and fast to prepare. The Stöber method is a well-known successful method for producing monodisperse SiO_2 spheres [114]. Moreover, SiO_2 has good solubility in based solution, making this compound easy to remove. In the final step, ammonia or sodium hydroxide solution was used to remove the SiO_2 core from SiO_2@TiO_2 by etching [95–97, 107]. Adding a hard alkaline solution to SiO_2@TiO_2 through sonication and stirring pushes high-

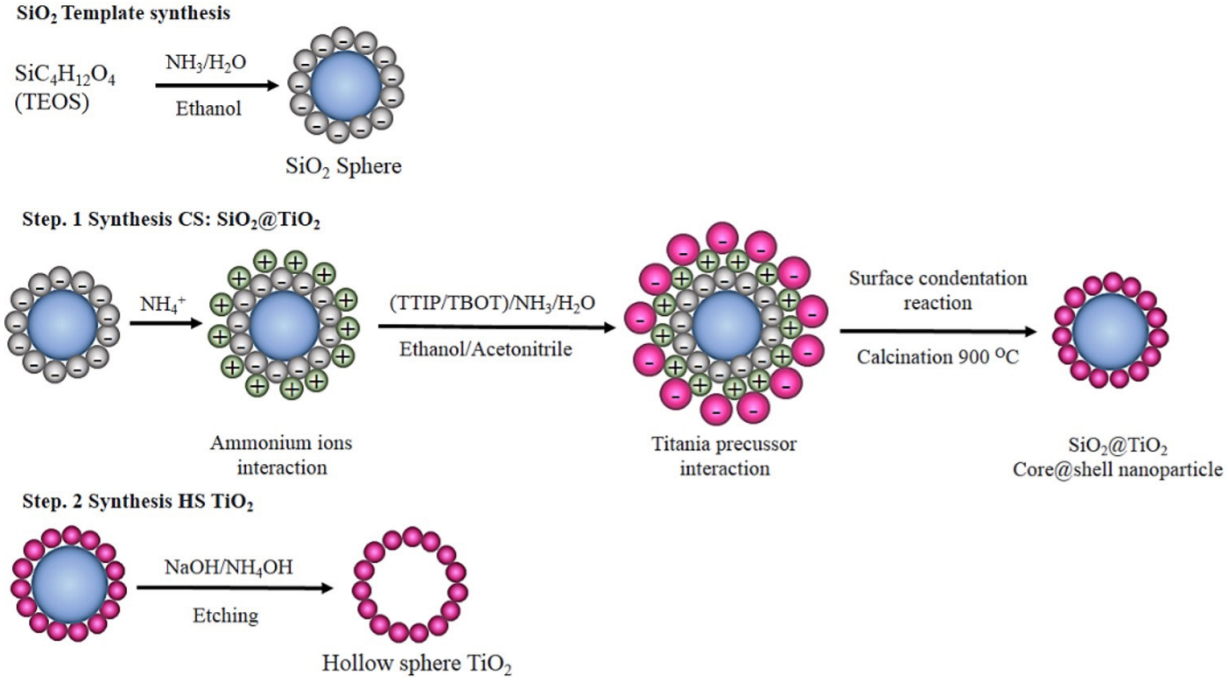

Figure 6. Schematic of two step HS TiO_2 synthesis *via* SiO_2@TiO_2.

intensity energy into the voids between the silica-titania, which causes partial etching of the silica core. Under conditions of strict induction reaction, it caused corrosion and etched silica-titania part. The etched silica and titania species are released into the solution and diffused from the nanosphere to the titania shell. Furthermore, the etched fragments undergo condensation and re-deposition on the titania shell's surface through Ostwald maturation (reverse reaction). This reversible reaction continues until a hollow nanosphere structure is formed [103]. The anatase phase of HS TiO_2 was obtained after calcination of SiO_2@ TiO_2 at 500-900°C [97,103,105]. Calcination at 900°C showed the optimal temperature of the anatase phase of HS TiO_2 [103]. At high temperatures, the slowing formation of the crystal structure of anatase HS TiO_2 occurs due to interaction with SiO_2 as a core [103].

Hollow sphere TiO_2 can also be synthesized with a hard template using gold (Au) from HAuCl and several inorganic salts (Table 2). The manufacture of HS TiO_2 with an Au template began with the formation of Au@TiO_2 resulting from the sol-gel method at more than 100°C. The HS TiO_2 was obtained by depositing the Au core with KCN [99]. The fabrication of HS TiO_2 has also been reported by Chen *et al.* [101] which uses the $CaCO_3$ template through a two-step reaction. The hollow sphere formation was obtained after etching $CaCO_3$ using HCl [101]. Lan *et al.* [100] reported the use of $K_3PW_{12}O_{40}$, obtained by mixing a solution of KCl and $H_3PW_{12}O_{40}$, as a template to produce HS TiO_2 with a diameter of 0.5-1 μm. The template was removed using 1 M NaOH solution [100]. Rakhman *et al.* [115] introduced a novel two-step synthesis method to fabricate HS TiO_2, achieving optimal crystallite sizes of 9.53 to 20.54 nm and micro-strains. The resulting hollow spheres demonstrated excellent photooxidative properties under UV irradiation, highlighting their potential for solar cell applications. Similarly, a one-pot sol-gel method has been applied for synthesizing HS TiO_2 embedded with silver nanoparticles (AgNPs), achieving uniform distribution of AgNPs on the HS TiO_2 and enhanced light harvesting for DSSCs [116].

Several existing synthesis methods have similar techniques for producing HS TiO_2 with different particle sizes. In the hydrothermal carbon-based templates and hard templates method, adding excess titania precursors was adopted to design HS TiO_2 with larger particle sizes. However, in the hydrothermal/solvothermal method, this approach will affect the cavity size of the HS TiO_2. The sol-gel method using a template can improve the shell's thickness in this situation. The template-assisted method also makes it possible to design the size of the HS TiO_2 cavity. Kanjana *et al.* [92] reported that the formation of HS TiO_2 with different particle sizes could be influenced by the pH and ratio of addition of the titania precursor to the solvent. The reaction at low pH (acidic) gave a larger particle size compared to neutral or alkaline conditions in the sol-gel carbon-based template synthesis [117].

In addition, other methods like co-precipitation and solid-state methods can also be used to synthesize HS TiO_2 [81,118]. However, this review focuses on the hydrothermal/solvothermal and sol-gel methods, as both these synthesis routes are the most popular among all.

3.3. Characterization of HS TiO_2

Scanning electron microscopy (SEM) and transmission electron microscopy (TEM) images are the primary data to determine the morphology of HS TiO_2. The data such as diameter size, particle size, grain size, crystal size, cavity, and shell thickness can also be obtained using both. Other data, such as binding energy curve by x-ray photoelectron spectroscopy (XPS), elemental mapping plot by energy dispersive X-ray spectroscopy (EDS), and absorption spectra by IR, were added by several researchers to provide information on reaction products at each stage, especially in the sol-gel method using templates. Interestingly, several articles discussed changes in the structure of the TiO_2 products to show the progress of the reaction. For example, Chen *et al.* [62] showed TEM images emphasizing the Kirkendall effect process (Figure 2) in producing HS TiO_2. Zhao *et al.* [119] studied the reaction rate of HS TiO_2 formation through Ostwald ripening (Figure 3) with TEM images.

Most of the characterization of HS TiO_2 by SEM and TEM through two-stage sol-gel synthesis presented different images of templates, intermediate materials, and hollow sphere products. In the carbon-based templates method, Song and Gao [85] presented a TEM images (Figure 7) of polystyrene (PS) sphere, PS@TiO_2, and HS SiO_2/TiO_2.

The PS ball template (Figure 7a) looks clear and smooth with a uniform size. The TiO_2 coating forming PS@TiO_2 (Figure 7b) shows a different image of the PS sphere with a rougher surface and larger particle size changes. Meanwhile, the HS SiO_2/TiO_2 formed after the removal of the PS core shows a smoother ring image than PS@TiO_2 (Figure 7c). Karabacak *et al.* [120] show the PS sphere's change to PS@ TiO_2 with the SEM image (Figure 8). Similar to the TEM image, the SEM image shows a smoother PS sphere surface of uniform size (Figure 8a) compared to PS@TiO_2, which offers a rougher surface (Figure 8b).

The formation of PS@TiO_2 as an intermediate for HS TiO_2 through a sol-gel pathway based on a carbon template was supported by IR spectroscopy. Shi *et al.* [121] confirmed the formation of PS@TiO_2 by comparing the IR spectra of PS, PS@TiO_2, and TiO_2 anatase. The difference in absorption bands of the three indicates the interaction of PS and TiO_2. The PS microspheres showed absorption bands around 3000 and 1470 cm^{-1}, representing the C-H and C-C stretchings of the phenyl group [121]. Absorption around 760 and 700 cm^{-1} was associated with bending vibrations of phenyl in the C-H and C-C groups. While the absorption at 650 cm^{-1} is related to solid Ti-O-Ti vibrations [121]. The production of HS TiO_2 by the sol-gel synthesis pathway using SiO_2 as the template was also confirmed *via* TEM images (Figure 9). The different solid structure of SiO_2@TiO_2 (Figure 9a) with ring-like HS TiO_2 (Figure 9b) followed by a change in the percentage of silica and titania in the EDS spectra indicated the success of dissolving the SiO_2 core by NaOH [36].

In addition to the primary data from TEM and SEM images, the formation of SiO_2@TiO_2 in several articles is shown by supporting data such as absorption spectra by fourier tranform infrared spectroscopy (FTIR), binding energy curve by XPS, and qualitative data on elemental percent by EDX (Table 3). The FTIR spectra specifically showed Si-O-Ti interaction on the formation of SiO_2@TiO_2 in the absorption area of 940-962 cm^{-1}. While the analysis of bond energy (B.E) with XPS on O1s measurements showed 2 to 3 peaks, with the characteristics of Ti-O-Ti at 527.6-530.2 eV, Ti-O-Si at 530.7-532.5 eV, and Si-O-Si at 531.5-533.3 eV. The SiO_2@TiO_2 characteristic is also shown in the reflectance

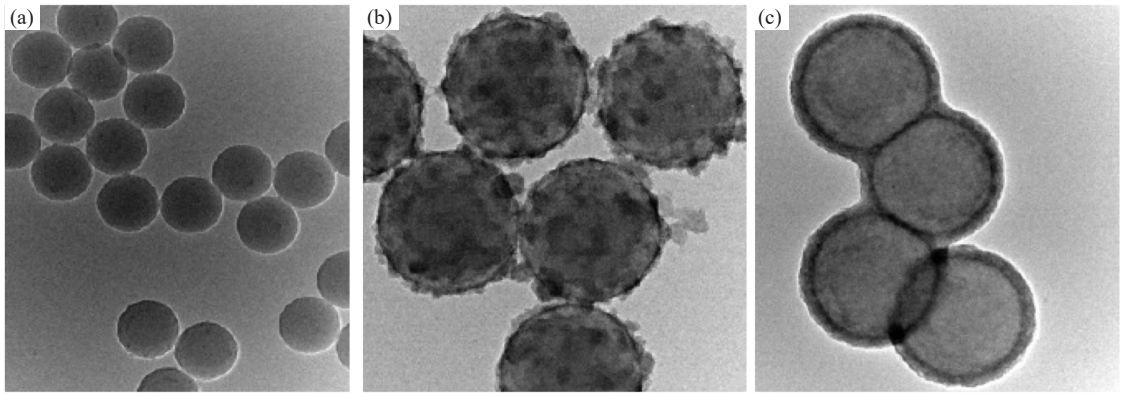

Figure 7. TEM images: (a) polystyrene (PS) spheres, (b) PS@TiO_2, (c) HS SiO_2/TiO_2 [85]. Licensed by American Chemical Society. TEM: Transmission electron microscopy.

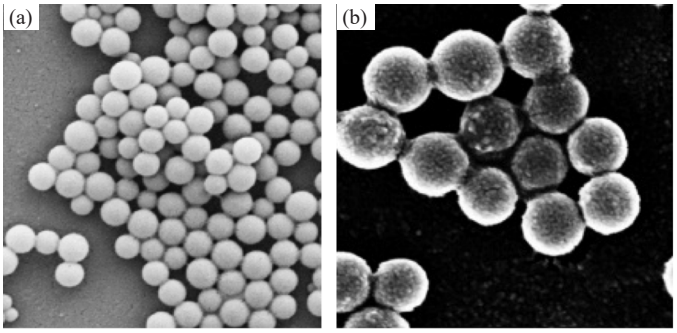

Figure 8. SEM images: (a) Polystyrene, (b) PS@TiO_2 [120]. Licensed by Elsevier.

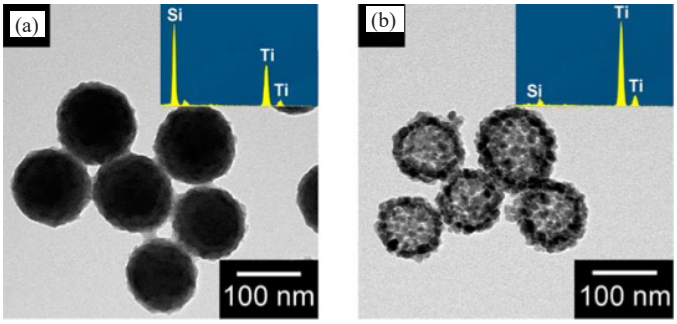

Figure 9. TEM images and EDS spectra (inset) of (a) SiO_2@TiO_2, (b) HS TiO_2 [36]. Licensed by American Chemical Society. TEM: Transmission electron microscopy.

and absorbance of UV/Vis spectra (Figure 5). The reflective index (*n*) of SiO_2@TiO_2 was between SiO_2 (1.47) dan TiO_2 (2.49) nanoparticles at 400-700 nm. Meanwhile, the UV/Vis SiO_2@TiO_2 absorption spectra showed higher adsorption than SiO_2 and TiO_2 nanoparticles at 400-650 nm [122].

4. Photovoltaic Characteristics

4.1. Scattering light ability of HS TiO_2

TEM image showing HS TiO_2 appears as a ring, indicating the presence of a cavity. It is a unique feature of HS TiO_2 in addition to the pores of the interface (intra-shell). This feature allows a strong internal light scattering in the HS TiO_2 compared to solid particles [98]. Lei *et al.* [123] investigated the light scattering properties of HS TiO_2 as indicated by the UV-Vis reflectance spectrum (Figure 10a). HS TiO_2 exhibits strong reflectance in the 400-800 nm range to more than 50%, while the TiO_2P25 is lower.

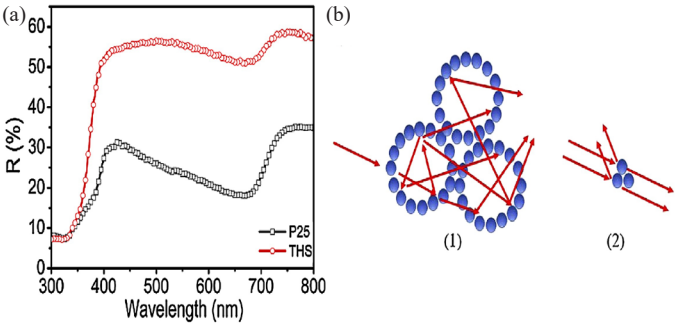

Figure 10. (a) DR UV-Vis spectra of the HS TiO_2 and TiO_2 P25 films. (b) A schematic light pathway illustration of [1] HS TiO_2 and [2] TiO_2 P25 nanoparticles [123]. Licensed by Elsevier.

In addition, HS TiO_2 also shows a stronger visible light absorption ability than TiO_2 P25 [69]. It is attributed to the ability of the hollow structure to absorb more photons than TiO_2 P25 [124]. The dye loading on HS TiO_2 also showed a higher amount than TiO_2 P25. However, dye-sensitized TiO_2 HS was able to maintain a higher reflectance than TiO_2 P25 [77]. This condition is associated with a greater opportunity for the dye to absorb photons [26]. The multi-reflection effect arises from HS TiO_2 to scatter incident light at different wavelengths in the visible area, and the scattering effect can increase the optical path of the incident light (Figure 10b). This condition contributes to higher light-harvesting efficiency to increase photocurrent density (*Jsc*) [123].

4.2. Photovoltaic performance

As mentioned earlier, the unique feature of HS TiO_2 is a distinct advantage in photovoltaic characteristics. Lee *et al.* [125] reported that the structural effect of HS TiO_2 was important, where HS TiO_2 showed better light absorption compared to the same particles after crushing into powders with a size of 10 nm. Despite having the same band gap at 3.2 eV as anatase TiO_2, the diameter and thickness of the HS TiO_2 shell were different, indicating different visible light absorption activities in

Table 3. Characterization of SiO_2@TiO_2.

FTIR	XPS B.E. (eV)						SEM/FESEM/TEM/HRTEM				EDX	References
Ti-O-Si	Si 2p	O 1s			Ti 2p		Particle size (nm)	Crystallite size (nm)	Core size (nm)	Shell thickness (nm)	Si:Ti (%)	
(cm^{-1})	Si-O-Si	Ti-O-Ti	Ti-O-Si	Si-O-Si	Ti 2p1/2	Ti 2p3/2						
940		529.9	532.5	533			~440 - ~560					[126]
							40					[114]
							110, 240, 530				46:54, 80:20, 92:8	[122]
							200, 260, 300, 320, 370					[127]
							81.2, 101.6, 124.4, 152.5				55.54:44.46	[128]
	101.8			531.5			~130					[129]
							225, 245, 250, 265	4.4, 4.5, 4.3, 4.6	200	23, 25, 34, 33		[130]
962		530.1	531.9	532.9	464.4	458.8		14.85	~310			[131]
943		530.2	531.9	532.6	464.2	458.6	450-550		~310			[132]
402								~7			38.60:1.15, 42.09:7.53, 25.29:14.49	[133]
	102.7				464.2	458.8	390			65		[23]
955								18.18, 18.26, 22.75, 28.98, 38.18	221	7, 17, 25	36.6:0.92, 36.02:1.56, 28.22:2.91	[134]
	101.41	527.63	530.73		462.13	456.18						[135]
	104.2	530.2	531.6	533.3			222		193			[136]
	103.9			533	464.1	458.4			100	0.35		[137]

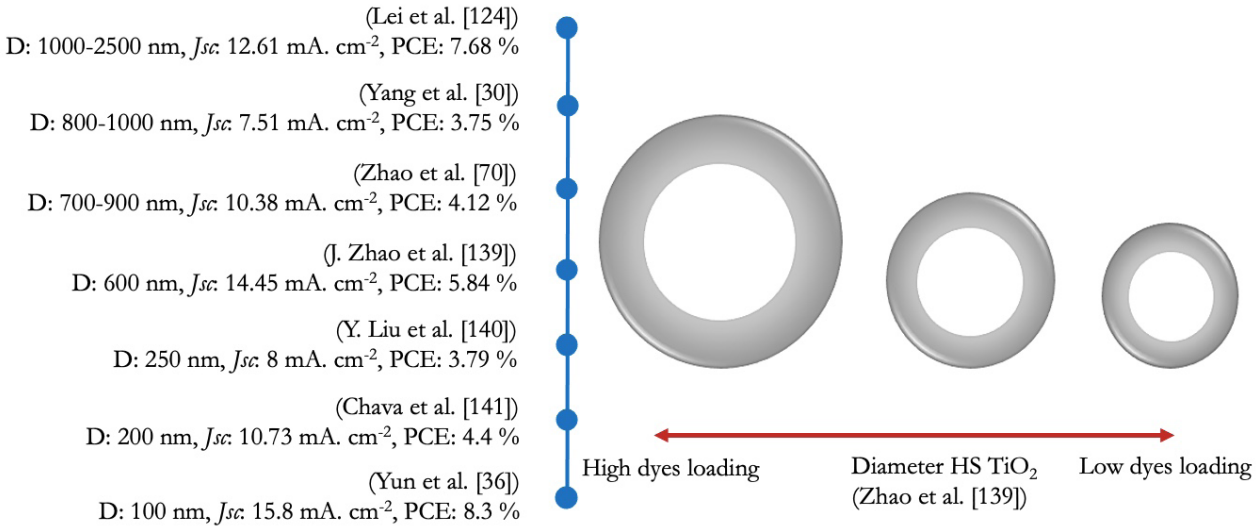

Figure 11. Effect of HS TiO_2 diameter on photovoltaic properties [30,36,70,124,139-141].

the 400-800 nm area. This condition confirms that the morphology of HS TiO_2 has a different effect on its photoactivity [106]. The HS TiO_2 with a diameter of ~100 nm provided the best PCE [36]. In addition to that, the diameter of the HS TiO_2 also affects the dye loading ability (Figure 11), where a larger HS TiO_2 diameter caused a reduction in the amount of dye loading [138]. This condition is thought to occur when light incident on the surface of the material experiences an extension of the wavelength path in the cavity, enhancing photon capture by dye molecules [36,99]. The large surface area of particles allows the dye loading to be higher than the solid particles, thus encouraging more optimal photon harvesting [98].

The higher photon absorption of HS TiO_2 is indicated by a decrease in wavelength (350-800 nm) in the transmittance spectrum [99]. This phenomenon is associated with the efficiency of current conduction (electron transfer) from the dye by HS TiO_2 to the DSSC system [26]. This indication is seen in the pore characteristics and surface area of the material that affect the loading ability of the dye molecules and the electron transfer speed of the dye molecules [26].

4.3. Enhancing photovoltaic characteristic

Modifications of HS TiO_2 as a semiconductor component in DSSC have been reported to enhance the *Jsc* and PCE (Table 4). It is reported that the combination of HS TiO_2 and TiO_2 nanosheets enhanced *Jsc* by 2.44% and PCE by 0.96% [119]. Meanwhile, HS TiO_2 composite films with TiO_2 nanotube arrays enhanced *Jsc* by 3.05%, with a 1.31% improvement in PCE [140]. Adding non-semiconductor materials such as carbon nanotubes enhanced *Jsc* by 1.6% and PCE by 0.77% [141]. Meanwhile, 0.25 mol% Fe doping on HS TiO_2 increased *Jsc* by 4.84% and PCE by 2.39% at the optimum conditions, which have the surface area and dye loading of 122.84 $m^2 g^{-1}$ and 22.12×10^{-8} mol cm^{-2}, respectively [142]. Additionally, a study reported that DSSCs fabricated with Fe/S–TiO_2 photoanodes exhibited an improved solar-to-electrical energy conversion efficiency of 6.46%, compared to 3.43% for pure TiO_2, under full sunlight illumination [143].

Another modification is the addition of localized surface plasmon resonance material (LSPRM), such as Au, Ag, or alloys of both, which increased the PCE by 0.5, 0.7, and 1.1 %, respectively [141]. The addition of Ag with a larger particle size gave an even higher PCE of 1.9 % [98]. According to Song *et al.* [144], LSPRM in the DSSC system increased the number of electrons released from the dye and the electron density of the semiconductor. The interfacial interaction between LSPRM and the semiconductor causes a fast electron transfer from the dye molecule [145]. The plasmon effect can be formed when the light comes in and stimulates free electron oscillations in LSPRM [146]. When the LSPRM on the surface of the semiconductor material is excited by light, a strong electromagnetic field is generated. A strong electromagnetic field can enhance the photocurrent and regeneration of photoelectrons [147]. However, the addition of a higher concentration of LSPRM could attenuate the efficiency of the DSSC due to a decrease in dye loading on the TiO_2 semiconductor [146]. Enhancing the local electromagnetic field around the nanostructure is the key to increasing dye adsorption in the DSSC system [148]. LSPRM plays multiple roles in the performance of DSSCs, including an enhancement in the dye adsorption coefficient and optical absorption due to surface plasmonic resonance [149]. LSPRM also acts as an electron sink for charge carriers on photoinduction, enhancing the interfacial electron transfer process and minimizing electron transfer recombination, thereby enhancing the electron transfer process in DSSC [148].

HS TiO_2 has demonstrated excellent photovoltaic performance under laboratory conditions. However, several challenges might hinder its practical applications. One significant challenge is the stability and durability of HS TiO_2 structures. Over time, environmental factors such as moisture, UV radiation, and temperature fluctuations can lead to degradation, resulting in a decline in photovoltaic performance. Implementing protective coatings or encapsulation techniques can shield HS TiO_2 structures from these environmental stressors [150]. Manufacturing scalability is another concern. The synthesis of HS TiO_2 structures often involves complex processes that may not be easily scalable for large-scale production [151]. Therefore, scaled-up productions of HS TiO_2 in order to establish the best performance and cost-effective synthesis route is required.

Table 4. Modifications of HS TiO_2 for DSSC.

Modifications	Enhancement of *Jsc* (%)	Enhancement of *Voc* (%)	Enhancement of PCE (%)	References
Film composite HS TiO_2/carbon nanotubes	1.6	0.013	0.77	[141]
Double light-scattering layer HS TiO_2 and nanosheet TiO_2	2.44	0	0.96	[119]
TiO_2 HS/TiO_2 nanotube array composite films	3.05	-0.01	1.31	[140]
TiO_2 HS assembly from nanosheets	3.99	-0.01	2.22	[30]
Fe-doped TiO_2 HS	4.845	0.038	2.39	[142]
HS TiO_2 decorated small Ag NP	3.1	0	1.2	[98]
HS TiO_2 decorated large Ag NP	4.3	0	1.9	
HS TiO_2 decorated Ag NP	1	0.01	0.7	[36]
HS TiO_2 decorated Au NP	0.5	0.01	0.5	
HS TiO_2 decorated Au@ Ag NP	1.5	0.01	1.1	

The addition of LSPRM to HS TiO_2 provides an opportunity to enhance the efficiency of the DSSC compared to the single semiconductor material in the photoanode. It provides a better prospect for DSSC development [36]. Thus, it raises several new challenges to conduct morphological tracing and suitable LSPRM arrangement on HS TiO_2-based photoanode components to increase the work conversion efficiency (PCE) of DSSC.

5. Conclusions and Outlooks

Developing HS TiO_2 as a semiconductor material for DSSC components is important for improving the efficiency of DSSC. HS TiO_2 offers significant morphological advantages, which can improve the PCE of DSSC. The unique morphology of HS TiO_2 contributes to improved short-circuit current density (*Jsc*) and, consequently, a higher PCE. This review highlights the synthesis of HS TiO_2 and its photovoltaic properties as key areas of innovation.

This review presents several HS TiO_2 synthesis methods, such as hydrothermal/solvothermal, sol-gel by carbon-based template, and hard template. Hydrothermal/solvothermal has the advantages over these methods because it has the shortest synthesis route compared to the sol-gel method for the formation of the HS TiO_2 structure as well as the arrangement of the crystal phase. Meanwhile, the fabrication of HS TiO_2 through the hard template sol-gel method can provide a smaller pore size than other synthesis pathways. The uniqueness of HS TiO_2 pores, smaller particle size, and large surface area allow the acceleration of electron transfer from the dye to the device and show a higher *Jsc* than other morphologies. Although the HS TiO_2 from the SiO_2@TiO_2 produced smaller particle sizes and higher PCE compared to other pathways, the synthesis of this pathway requires the longest fabrication time starting from the formation of SiO_2@TiO_2, then the growth of the crystal phase by calcination, and followed by the removal of the SiO_2 core through etching.

Hollow sphere TiO_2 can scatter light very well due to the influence of its micropore particles and the uniqueness of its cavity. This property is the advantage of HS TiO_2 for photocatalyst applications and solar cells. Especially in DSSC applications, semiconductor HS TiO_2 has several challenges, including the loading dye capacity and the electron transfer rate, which still depend on the particle size of the HS TiO_2. The particle size of HS TiO_2 is one of the variables studied for its ability as a dye adsorbent, incident light scattering properties, and electron transfer speed in DSSC applications. So far, the thickness of the HS TiO_2 shell has not received similar attention in these studies. According to Mie's theory, the thickness of the HS TiO_2 shell can affect the scattering of incident light. In the future, therefore, the thickness of the HS TiO_2 shell would be the other key parameter affecting the conversion of light into electricity in DSSC.

Recent advancements in DSSCs have focused on enhancing the dye loading and light-harvesting efficiency through various material modifications. Incorporating carbon nanotubes (CNTs) into the photoanode has been shown to improve electron transport and reduce recombination rates. For instance, research demonstrated that integrating multi-walled carbon nanotubes (MWCNTs) into the $BaTiO_3$ photoelectrode led to improved photovoltaic performance. Additionally, doping TiO_2 with elements like iron (Fe) has been found to enhance the material's surface area and electronic properties.

The incorporation of LSPRM, such as silver or gold nanoparticles, has been extensively investigated to enhance light absorption and facilitate faster electron injection in DSSCs. These nanoparticles generate strong localized surface plasmon resonance (LSPR) fields, which can significantly enhance the photonic absorption of dyes. In the future, the composition and construction of the thin layer system, elemental doping, and the addition of LSPRM to HS TiO_2-based photoanode will become promising studies in developing more efficient DSSC.

Credit authorship contribution statement

Khusna Arif Rakhman: Data curation, Investigation, Methodology, Writing – original draft. **Nurul Hidayat Aprilita:** Formal analysis, Supervision, Writing – review & editing. Rohana **Adnan:** Formal analysis, Methodology, Writing – review & editing. **Indriana Kartini:** Funding acquisition, Methodology, Supervision, Writing – review & editing.

Declaration of competing interest

The authors declare that they have no known financial interests in the work reported in this paper.

Declaration of generative AI and AI-assisted technologies in the writing process

The authors confirm that there was no use of artificial intelligence (AI)-assisted technology for assisting in the writing or editing of the manuscript and no images were manipulated using AI.

References

1. Zhang, P., Hu, Z., Wang, Y., Qin, Y., Sun, X.W., Li, W., Wang, J., 2016. Enhanced photovoltaic properties of dye-sensitized solar cell based on ultrathin 2D TiO_2 nanostructures. *Applied Surface Science*, **368**, 403-8. https://doi.org/10.1016/j.apsusc.2016.02.010
2. Wu, W.Q., Xu, Y.F., Rao, H.S., Su, C.Y., Kuang, D.B., 2014. Trilayered photoanode of TiO2 nanoparticles on a 1D-3D nanostructured TiO_2-grown flexible Ti substrate for high-efficiency (9.1%) dye-sensitized solar cells with unprecedentedly high photocurrent density. *The Journal of Physical Chemistry C*, **118**, 16426–16432. https://doi.org/10.1021/jp4116782
3. Basu, K., Benetti, D., Zhao, H., Jin, L., Vetrone, F., Vomiero, A., Rosei, F., 2016. Enhanced photovoltaic properties in dye sensitized solar cells by surface treatment of SnO_2 photoanodes. *Scientific Reports*, **6**, 23312. https://doi.org/10.1038/srep23312
4. Ghann, W., Kang, H., Sheikh, T., Yadav, S., Chavez-Gil, T., Nesbitt, F., Uddin, J., 2017. Fabrication, optimization and characterization of natural dye sensitized solar cell. *Scientific Reports*, **7**, 41470. https://doi.org/10.1038/srep41470
5. Omar, A., Ali, M.S., Abd Rahim, N., 2020. Electron transport properties analysis of titanium dioxide dye-sensitized solar cells (TiO_2-DSSCs) based natural dyes using electrochemical impedance spectroscopy concept: A review. *Solar Energy*, **207**, 1088-1121. https://doi.org/10.1016/j.solener.2020.07.028
6. Karim, N.A., Mehmood, U., Zahid, H.F., Asif, T., 2019. Nanostructured photoanode and counter electrode materials for efficient dye-sensitized solar cells (DSSCs). *Solar Energy*, **185**, 165-188. https://doi.org/10.1016/j.solener.2019.04.057
7. Hosseinnezhad, M., Gharanjig, K., Yazdi, M.K., Zarrintaj, P., Moradian, S., Saeb, M.R., Stadler, F.J., 2020. Dye-sensitized solar cells based on natural photosensitizers: A green view from Iran. *Journal of Alloys and Compounds*, **828**, 154329. https://doi.org/10.1016/j.jallcom.2020.154329
8. Molaeirad, A., Janfaza, S., Karimi-Fard, A., Mahyad, B., 2015. Photocurrent generation by adsorption of two main pigments of halobacterium salinarum on TiO_2 nanostructured electrode. *Biotechnology and Applied Biochemistry*, **62**, 121-5. https://doi.org/10.1002/bab.1244
9. Sirotkin, N., Khlyustova, A., Belikova, J., 2023. Fabrication of dye-Sensitized solar cells based on novel mixed tungsten–Molybdenum and tungsten–Titanium oxides nanoparticles prepared by impulse underwater plasma. *Physica Status Solidi (a)*, **220**, 2200435.. https://doi.org/10.1002/pssa.202200435
10. Yusuf, S.N.F., Aziz, M.F., Hassan, H.C., Bandara, T.M.W.J., Mellander, B.-E., Careem, M.A., Arof, A.K., 2014. Phthaloylchitosan-based gel polymer electrolytes for efficient dye-sensitized solar cells. *Journal of Chemistry*, **2014**, 1-8. https://doi.org/10.1155/2014/783023
11. Majumdar, S., Mondal, A., Mahajan, A., Bhattacharya, S.K., Ray, R., 2023. Dye-sensitized solar cell employing chitosan-based biopolymer electrolyte. *IOP Conference Series: Materials Science and Engineering*, **1291**, 012014. https://doi.org/10.1088/1757-899x/1291/1/012014
12. Mubeen, S., Lee, J., Lee, W.R., Singh, N., Stucky, G.D., Moskovits, M., 2014. On the plasmonic photovoltaic. *ACS Nano*, **8**, 6066-6073. https://doi.org/10.1021/nn501379r
13. Song, J.-L., Wang, X., Wong, C.C., 2015. Simple preparation of fluorine-doped TiO_2 photoanode for high performance dye sensitized solar cells. *Electrochimica Acta*, **173**, 834-8. https://doi.org/10.1016/j.electacta.2015.05.118
14. Ahmad, M.S., Rahim, N.A., Pandey, A.K., 2018. Improved electron transfer of TiO_2 based dye sensitized solar cells using Ge as sintering aid. *Optik*, **157**, 134-140. https://doi.org/10.1016/j.ijleo.2017.11.073
15. Bai, Y., Mora-Seró, I., De Angelis, F., Bisquert, J., Wang, P., 2014. Titanium dioxide nanomaterials for photovoltaic applications. *Chemical Reviews*, **114**, 10095-10130. https://doi.org/10.1021/cr400606n
16. Barea, E.M., Bisquert, J., 2013. Properties of chromophores determining recombination at the TiO_2–dye–electrolyte interface. *Langmuir*, **29**, 8773–8781.
17. Li, G., Sheng, L., Li, T., Hu, J., Li, P., Wang, K., 2019. Engineering flexible dye-sensitized solar cells for portable electronics. *Solar Energy*, **177**, 80-98. https://doi.org/10.1016/j.solener.2018.11.017
18. Boro, B., Gogoi, B., Rajbongshi, B.M., Ramchiary, A., 2018. Nano-structured TiO_2/ZnO nanocomposite for dye-sensitized solar cells application: A review. *Renewable and Sustainable Energy Reviews*, **81**, 2264-2270. https://doi.org/10.1016/j.rser.2017.06.035

19. Babar, F., Mehmood, U., Asghar, H., Mehdi, M.H., Khan, A.U.H., Khalid, H., Huda, N.ul, Fatima, Z., 2020. Nanostructured photoanode materials and their deposition methods for efficient and economical third generation dye-sensitized solar cells: A comprehensive review. *Renewable and Sustainable Energy Reviews*, **129**, 109919. https://doi.org/10.1016/j.rser.2020.109919
20. Taleb, A., Mesguich, F., Hérissan, A., Colbeau-Justin, C., Yanpeng, X., Dubot, P., 2016. Optimized TiO_2 nanoparticle packing for DSSC photovoltaic applications. *Solar Energy Materials and Solar Cells*, **148**, 52-9. https://doi.org/10.1016/j.solmat.2015.09.010
21. Jeng, M.J., Wung, Y.L., Chang, L.B., Chow, L., 2013. Particle size effects of TiO_2 layers on the solar efficiency of dye-sensitized solar cells. *International Journal of Photoenergy*, 2013. https://doi.org/10.1155/2013/563897
22. Archana, T., Vijayakumar, K., Arivanandhan, M., Jayavel, R., 2019. TiO_2 nanostructures with controlled morphology for improved electrical properties of photoanodes and quantum dot sensitized solar cell characteristics. *Surfaces and Interfaces*, **17**, 100350. https://doi.org/10.1016/j.surfin.2019.100350
23. Ma, J., Guo, X., Ge, H., Tian, G., Zhang, Q., 2018. Seed-mediated photodeposition route to ag-decorated SiO_2@TiO_2 microspheres with ideal core-shell structure and enhanced photocatalytic activity. *Applied Surface Science*, **434**, 1007-1014. https://doi.org/10.1016/j.apsusc.2017.11.020
24. Maurya, I.C., Senapati, S., Singh, S., Srivastava, P., Maiti, P., Bahadur, L., 2018. Effect of particle size on the performance of TiO_2 based dye-sensitized solar cells. *Chemistry Select*, **3**, 9872–9880. https://doi.org/10.1002/slct.201801745
25. Ran, H., Fan, J., Zhang, X., Mao, J., Shao, G., 2018. Enhanced performances of dye-sensitized solar cells based on Au-TiO_2 and Ag-TiO_2 plasmonic hybrid nanocomposites. *Applied Surface Science*, **430**, 415-423. https://doi.org/10.1016/j.apsusc.2017.07.107
26. Liu, Q., Wang, J., 2019. Dye-sensitized solar cells based on surficial TiO_2 modification. *Solar Energy*, **184**, 454-465. https://doi.org/10.1016/j.solener.2019.04.032
27. Devadiga, D., Selvakumar, M., Shetty, P., Santosh, M.S., 2021. Recent progress in dye sensitized solar cell materials and photo-supercapacitors: A review. *Journal of Power Sources*, **493**, 229698. https://doi.org/10.1016/j.jpowsour.2021.229698
28. González-Verjan, V.A., Trujillo-Navarrete, B., Félix-Navarro, R.M., de León, J.N.D., Romo-Herrera, J.M., Calva-Yáñez, J.C., Hernández-Lizalde, J.M., Reynoso-Soto, E.A., 2020. Effect of TiO_2 particle and pore size on DSSC efficiency. *Materials for Renewable and Sustainable Energy*, **9**. https://doi.org/10.1007/s40243-020-00173-7
29. Kwoka, M., Galstyan, V., Comini, E., Szuber, J., 2017. Pure and highly Nb-doped titanium dioxide nanotubular arrays: Characterization of local surface properties. *Nanomaterials (Basel, Switzerland)*, **7**, 456. https://doi.org/10.3390/nano7120456
30. Yang, R., Cai, J., Lv, K., Wu, X., Wang, W., Xu, Z., Li, M., Li, Q., Xu, W., 2017. Fabrication of TiO_2 hollow microspheres assembly from nanosheets (TiO_2-HMSs-NSs) with enhanced photoelectric conversion efficiency in DSSCs and photocatalytic activity. *Applied Catalysis B: Environmental*, **210**, 184-193. https://doi.org/10.1016/j.apcatb.2017.03.064
31. Shivaramu, N.J., Divya, J., Coetsee, E., Swart, H.C., 2024. Metal oxides for dye-sensitized solar cells. In: Metal Oxides for next-generation optoelectronic, photonic, and photovoltaic applications. Elsevier; p. 543-576. https://doi.org/10.1016/B978-0-323-99143-8.00017-1
32. Liu, H., Ma, H., Joo, J., Yin, Y., 2016. Contribution of multiple reflections to light utilization efficiency of submicron hollow TiO_2 photocatalyst. *Science China Materials*, **59**, 1017-1026. https://doi.org/10.1007/s40843-016-5127-7
33. Fu, N., Jiang, X., Chen, D., Duan, Y., Zhang, G., Chang, M., Fang, Y., Lin, Y., 2019. Au/TiO_2 nanotube array based multi-hierarchical architecture for highly efficient dye-sensitized solar cells. *Journal of Power Sources*, **439**, 227076. https://doi.org/10.1016/j.jpowsour.2019.227076
34. Gao, Q., Zhang, X., Duan, L., Li, X., Lü, W., 2019. Au nanoparticle-decorated urchin-like TiO_2 hierarchical microspheres for high performance dye-sensitized solar cells. *Superlattices and Microstructures*, **129**, 185-192. https://doi.org/10.1016/j.spmi.2019.03.028
35. Li, Y., Zhou, Y., Wang, Y., Zhou, R., Ling, Q., Niu, H., Zhang, W., Wang, C., Qiu, J., Guo, Z., Xu, J., 2019. Au nanoparticle-decorated urchin-like TiO_2 hierarchical microspheres for high performance dye-sensitized solar cells. *Electrochimica Acta*, **293**, 230-9. https://doi.org/10.1016/j.electacta.2018.10.035
36. Yun, J., Hwang, S.H., Jang, J., 2015. Fabrication of Au@Ag core/shell nanoparticles decorated TiO_2 hollow structure for efficient light-harvesting in dye-sensitized solar cells. *ACS Applied Materials & Interfaces*, **7**, 2055-2063. https://doi.org/10.1021/am508065n
37. Jafri, N.N.M., Jaafar, J., Aziz, F., Salleh, W.N.W., Yusof, N., Othman, M.H.D., Rahman, M.A., Ismail, A.F., Rahman, R.A., Khongnakorn, W., 2022. Development of free-standing titanium dioxide hollow nanofibers photocatalyst with enhanced recyclability. *Membranes*, **12**, 342. https://doi.org/10.3390/membranes12030342
38. Xiao, M., Wang, Z., Lyu, M., Luo, B., Wang, S., Liu, G., Cheng, H.M., Wang, L., 2019. Hollow nanostructures for photocatalysis: Advantages and challenges. *Advanced materials (Deerfield Beach, Fla.)*, **31**, e1801369. https://doi.org/10.1002/adma.201801369
39. Zhang, P., Lou, X.W.(David), 2019. Design of heterostructured hollow photocatalysts for solar-to-chemical energy conversion. *Advanced Materials*, **31**. https://doi.org/10.1002/adma.201900281
40. Zhang, G., Chen, D., Li, N., Xu, Q., Li, H., He, J., Lu, J., 2020. Construction of hierarchical hollow Co9 S8 /ZnIn2 S4 tubular heterostructures for highly efficient solar energy conversion and environmental remediation. *Angewandte Chemie (International ed. in English)*, **59**, 8255-8261. https://doi.org/10.1002/anie.202000503
41. Fang, B., Xing, Z., Sun, D., Li, Z., Zhou, W., 2022. Hollow semiconductor photocatalysts for solar energy conversion. *Advanced Powder Materials*, **1**, 100021. https://doi.org/10.1016/j.apmate.2021.11.008
42. Tamilselvan, S.N., Shanmugan, S., 2024. Towards sustainable solar cells: Unveiling the latest developments in bio-nano materials for enhanced DSSC efficiency. *Clean Energy*, **8**, 238-257. https://doi.org/10.1093/ce/zkae031
43. Korir, B.K., Kibet, J.K., Ngari, S.M., 2024. A review on the current status of dye-sensitized solar cells: Toward sustainable energy. *Energy Science & Engineering*, **12**, 3188–3226.
44. Xue, C., An, H., Shao, G., Yang, G., 2021. Accelerating directional charge separation *via* built-in interfacial electric fields originating from work-function differences. *Chinese Journal of Catalysis*, **42**, 583-594. https://doi.org/10.1016/s1872-2067(20)63649-x
45. Kim, N., Ju, S., Ha, J., Choi, H., Sung, H., Lee, H., 2022. Hierarchical co–Pi clusters/Fe_2O_3 nanorods/FTO micropillars 3D branched photoanode for high-performance photoelectrochemical water splitting. *Nanomaterials*, **12**, 3664. https://doi.org/10.3390/nano12203664
46. Liu, G., Li, N., Zhao, Y., Wang, M., Yao, R., Zhao, F., Wu, Y., Li, J., 2019. Porous versus compact hematite nanorod photoanode for high-performance photoelectrochemical water oxidation. *ACS Sustainable Chemistry & Engineering*, **7**, 11377-11385. https://doi.org/10.1021/acssuschemeng.9b01045
47. Shakeel, M., Pandey, A.K., Abd N., 2017. Advancements in the development of TiO_2 photoanodes and its fabrication methods for dye sensitized solar cell (DSSC) applications . A review. *Renewable and Sustainable Energy Reviews*, **77**, 89–108. https://doi.org/10.1016/j.rser.2017.03.129
48. Jafarzadeh, M., Sipaut, C.S., Dayou, J., Mansa, R.F., 2016. Recent progresses in solar cells: Insight into hollow micro/nano–structures. *Renewable and Sustainable Energy Reviews*, **64**, 543-568. https://doi.org/10.1016/j.rser.2016.06.028
49. Liu, Y.-Y., Ye, X.-Y., Chen, H., Cao, Y.-F., Lei, B.-X., Sun, W., Sun, Z.-F., 2019. Self-templated synthesis of large-scale hierarchical anatase titania nanotube arrays on transparent conductive substrate for dye-sensitized solar cells. *Advanced Powder Technology*, **30**, 572-580. https://doi.org/10.1016/j.apt.2018.12.010
50. Young, J., Luo, X., Hyung, S., 2018. Microporous and mesoporous materials synergistic effects of inter- and intra-particle porosity of TiO_2 nanoparticles on photovoltaic performance of dye-sensitized solar cells. *Microporous and Mesoporous Materials*, **266**, 214–222. https://doi.org/10.1016/j.micromeso.2018.03.003
51. He, X., Liu, J., Zhu, M., Guo, Y., Ren, Z., Li, X., 2017. Preparation of hierarchical rutile TiO_2 microspheres as scattering centers for efficient dye-sensitized solar cells. *Electrochimica Acta*, **255**, 187-194. https://doi.org/10.1016/j.electacta.2017.09.158
52. Reghunath, S., Pinheiro, D., KR, S.D., 2021. A review of hierarchical nanostructures of TiO_2: Advances and applications. *Applied Surface Science Advances*, **3**, 100063.
53. Ko, S.H., Grigoropoulos, C.P., 2014. Hierarchical nanostructures for energy devices. The Royal Society of Chemistry.https://doi.org/10.1016/j.apsadv.2021.100063
54. He, X., Zhang, J., Guo, Y., Liu, J., Li, X., 2019. Hierarchical TiO_2 microspheres composed with nanoparticle-decorated nanorods for the enhanced photovoltaic performance in dye-sensitized solar cells. *RSC Advances*, **9**, 3056-3062. https://doi.org/10.1039/c8ra09145e
55. Tsai, M.-C., Lee, J.-Y., Chang, Y.-C., Yang, M.-H., Chen, T.-T., Chang, I.-C., Lee, P.-C., Chiu, H.-T., Lee, R.-K., Lee, C.-Y., 2014. Scattering resonance enhanced dye absorption of dye sensitized solar cells at optimized hollow structure size. *Journal of Power Sources*, **268**, 1-6. https://doi.org/10.1016/j.jpowsour.2014.06.015
56. Bao, Y., Kang, Q.ling, Ma, J.zhong, 2018. Structural regulation of hollow spherical TiO_2 by varying titanium source amount and their thermal insulation property. *Colloids and Surfaces A: Physicochemical and Engineering Aspects*, **537**, 69-75. https://doi.org/10.1016/j.colsurfa.2017.10.019
57. Bao, R., Li, R., Chen, C., Wu, H., Xia, J., Long, C., Li, H., 2019. Biotemplated synthesis of 3D rare earth–doped TiO_2 hollow spheres for photocatalytic application. *Journal of Physics and Chemistry of Solids*, **126**, 78-84. https://doi.org/10.1016/j.jpcs.2018.10.023
58. Chen, X., Mao, S.S., 2007. Titanium dioxide nanomaterials: Synthesis, properties, modifications and applications. *Chemical Reviews*, **107**, 2891–2959. https://doi.org/10.1021/cr0500535
59. Li, J., Zeng, H.C., 2007. Hollowing sn-doped TiO_2 nanospheres *via* ostwald ripening. *Journal of the American Chemical Society*, **129**, 15839-15847. https://doi.org/10.1021/ja073521w
60. Zhang, X., Wang, M., Ding, J., Deng, J., Ran, C., Yang, Z., 2014. The synthesis and mechanism exploration of europium-doped $LiYF_4$ micro-octahedron phosphors with multilevel interiors. *Dalton Transactions (Cambridge, England: 2003)*, **43**, 5453-5461. https://doi.org/10.1039/c3dt53087f
61. Wang, X., Li, Z., Shi, J., Yu, Y., 2014. One-Dimensional Titanium Dioxide Nanomaterials: Nanowires. *Chemical Reviews*, **114**, 9346–9384. https://doi.org/10.1021/cr400633s
62. Chen, S., Wang, H., Zhu, L., Li, J., Sun, J., 2014. Solvothermal synthesis of TiO_2 hollow nanospheres utilizing the kirkendall effect and their photocatalytic activities. *Applied Surface Science*, **321**, 86-93. https://doi.org/10.1016/j.apsusc.2014.09.197
63. Zhu, L., Liu, K., Li, H., Sun, Y., Qiu, M., 2013. Solvothermal synthesis of mesoporous TiO_2 microspheres and their excellent photocatalytic performance under simulated sunlight irradiation. *Solid State Sciences*, **20**, 8-14. https://doi.org/10.1016/j.solidstatesciences.2013.02.026
64. Niu, K.Y., Park, J., Zheng, H., Alivisatos, A.P., 2013. Revealing bismuth oxide hollow nanoparticle formation by the kirkendall effect. *Nano Letters*, **13**, 5715-5719. https://doi.org/10.1021/nl4035362
65. Fan, H.J., Gösele, U., Zacharias, M., 2007. Formation of nanotubes and hollow nanoparticles based on kirkendall and diffusion processes: A review. *Small (Weinheim an der Bergstrasse, Germany)*, **3**, 1660-1671. https://doi.org/10.1002/smll.200700382
66. Kitchamsetti, N., Payyavula, S., Cho, J.S., 2024. A review on hollow nanostructures, its derived composites: Preparation, structural control, alterations, and their utilization as an electrode for supercapacitors, rechargeable batteries and

electrocatalysis. *Journal of Energy Storage*, **98**, 113143. https://doi.org/10.1016/j.est.2024.113143
67. Yu, K., Ling, M., Liang, J., Liang, C., 2019. Their lithium storage and photocatalytic properties. *Chemical Physics*, **517**, 222–7. https://doi.org/10.1016/j.chemphys.2018.10.022
68. Song, J., Yang, H.B., Wang, X., Khoo, S.Y., Wong, C.C., Liu, X.W., Li, C.M., 2012. Improved utilization of photogenerated charge using fluorine-doped TiO_2 hollow spheres scattering layer in dye-sensitized solar cells. *ACS Applied Materials & Interfaces*, **4**, 3712–7. https://doi.org/10.1021/am300801f
69. Wang, R., Cai, X., Shen, F., 2013. Preparation of TiO_2 hollow microspheres by a novel vesicle template method and their enhanced photocatalytic properties. *Ceramics International*, **39**, 9465-9470. https://doi.org/10.1016/j.ceramint.2013.05.064
70. Zhao, Y., Pan, F., Li, H., Zhao, D., Liu, L., Xu, G.Q., Chen, W., 2013. Uniform mesoporous anatase−brookite biphase TiO_2 hollow sphere with high crystallinity *via* ostwald ripening. *The Journal of Physical Chemistry C*, **117**, 21718–21723. https://doi.org/10.1021/jp408322g
71. Zhang, H., Sheng, Y., Song, Y., Li, H., Huang, J., Zheng, K., Huo, Q., Xu, X., Zou, H., 2013. Uniform hollow TiO_2:Sm^{3+} spheres: Solvothermal synthesis and luminescence properties. *Powder Technology*, **239**, 403-8. https://doi.org/10.1016/j.powtec.2013.02.010
72. Tsai, M.-C., Lee, J.-Y., Chen, P.-C., Chang, Y.-W., Chang, Y.-C., Yang, M.-H., Chiu, H.-T., Lin, I.-N., Lee, R.-K., Lee, C.-Y., 2014. Effects of size and shell thickness of TiO_2 hierarchical hollow spheres on photocatalytic behavior: An experimental and theoretical study. *Applied Catalysis B: Environmental*, **147**, 499-507. https://doi.org/10.1016/j.apcatb.2013.09.033
73. Wang, Y., Zhu, S., Chen, X., Tang, Y., Jiang, Y., Peng, Z., Wang, H., 2014. One-step template-free fabrication of mesoporous ZnO/TiO_2 hollow microspheres with enhanced photocatalytic activity. *Applied Surface Science*, **307**, 263-271. https://doi.org/10.1016/j.apsusc.2014.04.023
74. Wang, R., Cai, X., Shen, F., 2014. TiO_2 hollow microspheres with mesoporous surface: Superior adsorption performance for dye removal. *Applied Surface Science*, **305**, 352-8. https://doi.org/10.1016/j.apsusc.2014.03.089
75. Li, Y.Y., Wang, J.G., Liu, X.R., Shen, C., Xie, K., Wei, B., 2017. Au/TiO_2 hollow spheres with synergistic effect of plasmonic enhancement and light scattering for improved dye-sensitized solar cells. *ACS Applied Materials & Interfaces*, **9**, 31691-8. https://doi.org/10.1021/acsami.7b04624
76. Li, J., Cui, H., Song, X., Wei, N., Tian, J., 2017. The high surface energy of NiO {110} facets incorporated into TiO_2 hollow microspheres by etching Ti plate for enhanced photocatalytic and photoelectrochemical activity. *Applied Surface Science*, **396**, 1539-1545. https://doi.org/10.1016/j.apsusc.2016.11.205
77. Ye, X.-Y., Gu, Y.-H., Chen, H., Cao, Y.-F., Liu, Y.-Y., Lei, B.-X., Sun, W., Sun, Z.-F., 2019. Non-aqueous preparation of anatase TiO_2 hollow microspheres for efficient dye-sensitized solar cells. *Advanced Powder Technology*, **30**, 2408-2415. https://doi.org/10.1016/j.apt.2019.07.023
78. Huang, L., Fu, W., Wang, S., Guo, Z.-an, Bala, H., Wang, X., Sun, G., Cao, J., Zhang, Z., 2019. Facile template-free route to synthesis visible light respensive hollow TiO_2 spheres. *Materials Letters*, **244**, 50-3. https://doi.org/10.1016/j.matlet.2019.02.055
79. Lee, D.-H., Park, K.-S., Lee, C.-G., Swain, B., 2020. Facile one-pot synthesis of surface-fluorinated TiO_2 hollow spheres with enhanced photocatalytic activity. *Journal of Photochemistry and Photobiology A: Chemistry*, **400**, 112654. https://doi.org/10.1016/j.jphotochem.2020.112654
80. Sun, W., Zheng, H., Ma, J., Xi, Z., Wang, B., Hao, C., 2020. Preparation and electrorheological properties of eggshell-like TiO_2 hollow spheres *via* one step template-free solvothermal method. *Colloids and Surfaces A: Physicochemical and Engineering Aspects*, **601**, 125055. https://doi.org/10.1016/j.colsurfa.2020.125055
81. Guo, R., Bao, Y., Kang, Q., Liu, C., Zhang, W., Zhu, Q., 2022. Solvent-controlled synthesis and photocatalytic activity of hollow TiO_2 microspheres prepared by the solvothermal method. *Colloids and Surfaces A: Physicochemical and Engineering Aspects*, **633**, 127931. https://doi.org/10.1016/j.colsurfa.2021.127931
82. Zhong, Z., Yin, Y., Gates, B., Xia, Y., 2000. Preparation of mesoscale hollow spheres of TiO_2 and SnO_2 by templating against crystalline arrays of polystyrene beads. *Advanced Materials*, **12**, 206-9. https://doi.org/10.1002/(sici)1521-4095(200002)12:3<206::aid-adma206>3.0.co;2-5
83. Cheng, X., Chen, M., Wu, L., Gu, G., 2006. Novel and facile method for the preparation of monodispersed titania hollow spheres. *Langmuir: The ACS Journal of Surfaces and Colloids*, **22**, 3858-3863. https://doi.org/10.1021/la0534221
84. Syoufian, A., Inoue, Y., Yada, M., Nakashima, K., 2007. Preparation of submicrometer-sized titania hollow spheres by templating sulfonated polystyrene latex particles. *Materials Letters*, **61**, 1572-5. https://doi.org/10.1016/j.matlet.2006.07.081
85. Song, X., Gao, L., 2007. Fabrication of hollow hybrid microspheres coated with silica/titania *via* sol-gel process and enhanced photocatalytic activities. *The Journal of Physical Chemistry C*, **111**, 8180–7.
86. Agrawal, M., Pich, A., Zafeiropoulos, N.E., Stamm, M., 2008. Fabrication of hollow titania microspheres with tailored shell thickness. *Colloid and Polymer Science*, **286**, 593-601. https://doi.org/10.1007/s00396-007-1833-3
87. Chattopadhyay, J., Rokkim, H., Bongmoon, S., Pak, D., 2008. Performance of tin doped titania hollow spheres as electrocatalysts for hydrogen and oxygen production in water electrolysis. *International Journal of Hydrogen Energy*, **33**, 3270-3280. https://doi.org/10.1016/j.ijhydene.2008.03.057
88. Liao, C.-Y., Wang, S.-T., Chang, F.-C., Wang, H.P., Lin, H.-P., 2014. Preparation of TiO_2 hollow spheres for DSSC photoanodes. *Journal of Physics and Chemistry of Solids*, **75**, 38-41. https://doi.org/10.1016/j.jpcs.2013.08.005
89. Tabari-Saadi, Y., Mohammadi, M.R., 2015. Efficient dye-sensitized solar cells based on carbon-doped TiO_2 hollow spheres and nanoparticles. *Journal of Materials Science: Materials in Electronics*, **26**, 8863-8876. https://doi.org/10.1007/s10854-015-3567-1
90. Bao, Y., Kang, Q.L., Ma, J.Z., Liu, C., 2017. Monodisperse hollow TiO_2 spheres for thermal insulation materials: Template-free synthesis, characterization and properties. *Ceramics International*, **43**, 8596-8602. https://doi.org/10.1016/j.ceramint.2017.03.155
91. Ma, H., Zheng, W., Yan, X., Li, S., Zhang, K., Liu, G., Jiang, L., 2020. Polydopamine-induced fabrication of Ag-TiO_2 hollow nanospheres and their application in visible-light photocatalysis. *Colloids and Surfaces A: Physicochemical and Engineering Aspects*, **586**, 124283. https://doi.org/10.1016/j.colsurfa.2019.124283
92. Kanjana, N., Maiaugree, W., Poolcharuansin, P., Laokul, P., 2020. Size controllable synthesis and photocatalytic performance of mesoporous TiO_2 hollow spheres. *Journal of Materials Science & Technology*, **48**, 105-113. https://doi.org/10.1016/j.jmst.2020.03.013
93. Zhang, B., Tong, Z., Pang, Y., Xu, H., Li, X., Ji, H., 2022. Design and electrospun closed cell structured SiO_2 nanocomposite fiber by hollow SiO_2/TiO_2 spheres for thermal insulation. *Composites Science and Technology*, **218**, 109152. https://doi.org/10.1016/j.compscitech.2021.109152
94. Oh, W.K., Kim, S., Choi, M., Kim, C., Jeong, Y.S., Cho, B.R., Hahn, J.S., Jang, J., 2010. Cellular uptake, cytotoxicity, and innate immune response of silica-titania hollow nanoparticles based on size and surface functionality. *ACS Nano*, **4**, 5301-13. https://doi.org/10.1021/nn100561e
95. Choi, M., Kim, C., Jeon, S.O., Yook, K.S., Lee, J.Y., Jang, J., 2011. Synthesis of titania embedded silica hollow nanospheres *via* sonication mediated etching and re-deposition. *Chemical communications (Cambridge, England)*, **47**, 7092-4. https://doi.org/10.1039/c1cc11185j
96. Chen, Z.H., Kim, C., Zeng, X.B., Hwang, S.H., Jang, J., Ungar, G., 2012. Characterizing size and porosity of hollow nanoparticles: SAXS, SANS, TEM, DLS, and adsorption isotherms compared. *Langmuir: The ACS Journal of Surfaces and Colloids*, **28**, 15350-15361. https://doi.org/10.1021/la302236u
97. Li, S., Chen, J., Zheng, F., Li, Y., Huang, F., 2013. Synthesis of the double-shell anatase-rutile TiO_2 hollow spheres with enhanced photocatalytic activity. *Nanoscale*, **5**, 12150-12155. https://doi.org/10.1039/c3nr04043g
98. Hwang, S.H., Shin, D.H., Yun, J., Kim, C., Choi, M., Jang, J., 2014. SiO_2-TiO_2 hollow nanoparticles decorated with Ag nanoparticles: enhanced visible light absorption and improved light scattering in dye-sensitized solar cells. *Chemistry*, **20**, 4439–4446. https://doi.org/10.1002/chem.201304522
99. Song, M.-K., Rai, P., Ko, K.-J., Jeon, S.-H., Chon, B.-S., Lee, C.-H., Yu, Y.-T., 2014. Synthesis of TiO_2 hollow spheres by selective etching of Au@TiO_2 core-shell nanoparticles for dye sensitized solar cell applications. *RSC Advances*, **4**, 3529–3935. https://doi.org/10.1039/C3RA45860A
100. Lan, J., Wu, X., Lü, K., Si, L., Deng, K., 2015. Fabrication of TiO_2 hollow microspheres using K3PW12O40 as template. *Chinese Journal of Catalysis*, **36**, 2237-2243. https://doi.org/10.1016/s1872-2067(15)60987-1
101. Chen, W., Takai, C., Khosroshahi, H.R., Fuji, M., Shirai, T., 2016. SiO_2/TiO_2 double-shell hollow particles: Fabrication and UV-Vis spectrum characterization. *Advanced Powder Technology*, **27**, 812–828. https://doi.org/10.1016/j.apt.2015.10.016
102. Chava, R.K., Raj, S., Yu, Y.-T., 2016. Synthesis and electrophoretic deposition of hollow-TiO_2 nanoparticles for dye sensitized solar cell applications. *Journal of Alloys and Compounds*, **672**, 212-222. https://doi.org/10.1016/j.jallcom.2016.02.164
103. Zheng, H., Svengren, H., Huang, Z., Yang, Z., Zou, X., Johnsson, M., 2018. Hollow titania spheres loaded with noble metal nanoparticles for photocatalytic water oxidation. *Microporous and Mesoporous Materials*, **264**, 147-150. https://doi.org/10.1016/j.micromeso.2018.01.012
104. Yoon, C.M., Ryu, J., Yun, J., Kim, Y.K., Jang, J., 2018. Synthesis of hierarchical silica/Titania hollow nanoparticles and their enhanced electroresponsive activity. *ACS Applied Materials & Interfaces*, **10**, 6570-9. https://doi.org/10.1021/acsami.7b18895
105. Yao, X., Hu, X., Zhang, W., Gong, X., Wang, X., Pillai, S.C., Dionysiou, D.D., Wang, D., 2020. Mie resonance in hollow nanoshells of ternary TiO_2-Au-CdS and enhanced photocatalytic hydrogen evolution. *Applied Catalysis B: Environmental*, **276**, 119153. https://doi.org/10.1016/j.apcatb.2020.119153
106. Razavi-Khosroshahi, H., Wenhao, S., Fuji, M., 2020. Synthesis of TiO_2 hollow nanoparticles with different shell thickness and effect of structure on photocatalytic activity. *Solid State Sciences*, **103**, 106179. https://doi.org/10.1016/j.solidstatesciences.2020.106179
107. Lyu, J., Zhou, L., Shao, J., Zhou, Z., Gao, J., Dong, Y., Wang, Z., Li, J., 2020. TiO_2 hollow heterophase junction with enhanced pollutant adsorption, light harvesting, and charge separation for photocatalytic degradation of volatile organic compounds. *Chemical Engineering Journal*, **391**, 123602. https://doi.org/10.1016/j.cej.2019.123602
108. Li, L., Chen, X., Xiong, X., Wu, X., Xie, Z., Liu, Z., 2021. Synthesis of hollow TiO_2@SiO_2 spheres *via* a recycling template method for solar heat protection coating. *Ceramics International*, **47**, 2678-2685. https://doi.org/10.1016/j.ceramint.2020.09.117
109. Schroer, M.A., Westermeier, F., Lehmkühler, F., Conrad, H., Schavkan, A., Zozulya, A.V., Fischer, B., Roseker, W., Sprung, M., Gutt, C., Grübel, G., 2016. Colloidal crystallite suspensions studied by high pressure small angle x-ray scattering. *The Journal of Chemical Physics*, **144**, 084903. https://doi.org/10.1063/1.4941563
110. Nguyen, D.T., Kim, K.-S., 2016. Self-development of hollow TiO_2 nanoparticles by chemical conversion coupled with ostwald ripening. *Chemical Engineering Journal*, **286**, 266-271. https://doi.org/10.1016/j.cej.2015.10.077
111. Li, H., Jia, Y., Feng, X., Li, J., 2017. Facile fabrication of robust polydopamine microcapsules for insulin delivery. *Journal of Colloid and Interface Science*, **487**, 12-9. https://doi.org/10.1016/j.jcis.2016.10.012

112. Fang, X., Yang, H., Wu, G., Li, W., Chen, H., Wang, M., 2009. Preparation and characterization of low density polystyrene/TiO_2 core-shell particles for electronic paper application. *Current Applied Physics*, **9**, 755–9. https://doi.org/10.1016/j.cap.2008.07.011
113. Zhao, T., Qian, R., Tang, Y., Yang, J., Dai, Y., Lee, W.I., Pan, J.H., 2020. Controllable Synthesis and Crystallization of Nanoporous TiO_2 Deep-Submicrospheres and Nanospheres *via* an Organic Acid-Mediated Sol – Gel Process. *Langmuir*, **36**, 7447–7555. https://doi.org/10.1021/acs.langmuir.0c01008
114. Kim, C., Choi, M., Jang, J., 2010. Nitrogen-doped SiO_2/TiO_2 core/shell nanoparticles as highly efficient visible light photocatalyst. *Catalysis Communications*, **11**, 378-382. https://doi.org/10.1016/j.catcom.2009.11.005
115. Rakhman, K.A., Aprilita, N.H., Kartini, I., 2023. Effect of annealing and etching times on anatase TiO_2 hollow sphere. *Molekul*, **18**, 273. https://doi.org/10.20884/1.jm.2023.18.2.7480
116. Rakhman, K.A., Budhyantoro, A., Aprilita, N.H., Kartini, I., 2024. One-pot synthesis of hollow sphere TiO_2/Ag nanoparticles co-sensitized with peonidin: Pelargonidin for dye-sensitized solar cells applications. *Journal of Materials Science: Materials in Electronics*, **35**, 1926. https://doi.org/10.1007/s10854-024-13693-z
117. Danks, A.E., Hall, S.R., Schnepp, Z., 2016. The evolution of 'sol–gel' chemistry as a technique for materials synthesis. *Materials Horizons*, **3**, 91–112. https://doi.org/10.1039/C5MH00260E
118. Kumar, A., Pandey, G., 2018. Different methods used for the synthesis of TiO_2 based nanomaterials: A review. *American Journal of Nano Research and Applications*, **6**, 1. https://doi.org/10.11648/j.nano.20180601.11
119. Zhao, L., Li, J., Shi, Y., Wang, S., Hu, J., Dong, B., Lu, H., Wang, P., 2013. Double light-scattering layer film based on TiO_2 hollow spheres and TiO_2 nanosheets: Improved efficiency in dye-sensitized solar cells. *Journal of Alloys and Compounds*, **575**, 168-173. https://doi.org/10.1016/j.jallcom.2013.02.045
120. Karabacak, R.B.Ü, Erdem, M., Yurdakal, S., Çimen, Y., Türk, H., 2014. Facile two-step preparation of polystyrene/anatase TiO_2 core/shell colloidal particles and their potential use as an oxidation photocatalyst. *Materials Chemistry and Physics*, **144**, 498-504. https://doi.org/10.1016/j.matchemphys.2014.01.026
121. Shi, F., Li, Y., Wang, H., Zhang, Q., 2012. Formation of core/shell structured polystyrene/anatase TiO_2 photocatalyst *via* vapor phase hydrolysis. *Applied Catalysis B: Environmental*, **123-124**, 123-133. https://doi.org/10.1016/j.apcatb.2012.04.032
122. Son, S., Hwang, S.H., Kim, C., Yun, J.Y., Jang, J., 2013. Designed synthesis of SiO_2/TiO_2 core/shell structure as light scattering material for highly efficient dye-sensitized solar cells. *ACS Applied Materials & Interfaces*, **5**, 4815-4820. https://doi.org/10.1021/am400441v
123. Lei, B.-X., Zhang, P., Qiao, H.-K., Zheng, X.-F., Hu, Y.-S., Huang, G.-L., Sun, W., Sun, Z.-F., Zhang, X.-X., 2014. A facile template-free route for synthesis of anatase TiO_2 hollow spheres for dye-sensitized solar cells. *Electrochimica Acta*, **143**, 129-134. https://doi.org/10.1016/j.electacta.2014.07.106
124. Tang, G., Liu, S., Tang, H., Zhang, D., Li, C., Yang, X., 2013. Template-assisted hydrothermal synthesis and photocatalytic activity of novel TiO_2 hollow nanostructures. *Ceramics International*, **39**, 4969-4974. https://doi.org/10.1016/j.ceramint.2012.11.093
125. Lee, J.-Y., Tsai, M.-C., Chen, P.-C., Chen, T.-T., Chan, K.-L., Lee, C.-Y., Lee, R.-K., 2015. Thickness effects on light absorption and scattering for nanoparticles in the shape of hollow spheres. *The Journal of Physical Chemistry C*, **119**, 25754-25760. https://doi.org/10.1021/acs.jpcc.5b08435
126. Lee, J.-W., Kong, S., Kim, W.-S., Kim, J., 2007. Preparation and characterization of SiO_2/TiO_2 core-shell particles with controlled shell thickness. *Materials Chemistry and Physics*, **106**, 39-44. https://doi.org/10.1016/j.matchemphys.2007.05.019
127. Wang, Y., Chen, E., Lai, H., Lu, B., Hu, Z., Qin, X., Shi, W., Du, G., 2013. Enhanced light scattering and photovoltaic performance for dye-sensitized solar cells by embedding submicron SiO_2/TiO_2 core/shell particles in photoanode. *Ceramics International*, **39**, 5407-5413. https://doi.org/10.1016/j.ceramint.2012.12.048
128. Lee J, Hwang SH, Yun J, Jang J. 2014. Fabrication of SiO_2/TiO_2 double-shelled hollow nanospheres with controllable size *via* Sol – Gel reaction and sonication-mediated etching. *ACS Applied Materials & Interfaces*, **6**, 15420-12426. https://doi.org/10.1021/am503957f
129. Yoon, C.M., Lee, S., Cheong, O.J., Jang, J., 2015. Enhanced electroresponse of alkaline earth metal-doped Silica/Titania spheres by synergetic effect of dispersion stability and dielectric property. *ACS Applied Materials & Interfaces*, **7**, 18977-18984. https://doi.org/10.1021/acsami.5b02388
130. Ullah, S., Ferreira-Neto, E.P., Pasa, A.A., Alcântara, C.C.J., Acuña, J.J.S., Bilmes, S.A., Martínez Ricci, M.L., Landers, R., Fermino, T.Z., Rodrigues-Filho, U.P., 2015. Enhanced photocatalytic properties of core@shell SiO_2@TiO_2 nanoparticles. *Applied Catalysis B: Environmental*, **179**, 333-343. https://doi.org/10.1016/j.apcatb.2015.05.036
131. Chang, M., Song, Y., Chen, J., Cui, L., Shi, Z., Sheng, Y., Zou, H., 2018. Photocatalytic and photoluminescence properties of core – shell SiO_2@TiO_2:Eu3+,Sm3+ and its etching products. *ACS Sustainable Chemistry & Engineering*, **6**, 223–236. https://doi.org/10.1021/acssuschemeng.7b02285
132. Chang, M., Song, Y., Chen, J., Cui, L., Sheng, Y., Shi, Z., Zou, H., 2017. SiO_2@TiO_2:Eu3+ and its derivatives: Design, synthesis, and properties. *Crystal Growth & Design*, **17**, 6486 – 6497. https://doi.org/10.1021/acs.cgd.7b01149
133. Kitsou, I., Panagopoulos, P., Maggos, T., Arkas, M., Tsetsekou, A., 2018. Development of SiO_2@TiO_2 core-shell nanospheres for catalytic applications. *Applied Surface Science*, **441**, 223-231. https://doi.org/10.1016/j.apsusc.2018.02.008
134. Wang, D., Tan, Y., Xu, H., Wang, X., Yu, L., Xiao, Z., Wang, J., Xu, S., 2019. A tough and fluorescent dual nanocomposite hydrogel based on SiO_2@TiO_2 core-shell nanoparticles. *Applied Surface Science*, **467-468**, 588-595. https://doi.org/10.1016/j.apsusc.2018.10.208
135. Wang, W., Chen, H., Fang, J., Lai, M., 2019. Large-scale preparation of rice-husk-derived mesoporous SiO_2@TiO_2 as efficient and promising photocatalysts for organic contaminants degradation. *Applied Surface Science*, **467-468**, 1187-1194. https://doi.org/10.1016/j.apsusc.2018.10.275
136. Ferreira-Neto, E.P., Ullah, S., Simões, M.B., Perissinotto, A.P., de Vicente, F.S., Noeske, P.-L.M., Ribeiro, S.J.L., Rodrigues-Filho, U.P., 2019. Solvent-controlled deposition of titania on silica spheres for the preparation of SiO_2@TiO_2 core@shell nanoparticles with enhanced photocatalytic activity. *Colloids and Surfaces A: Physicochemical and Engineering Aspects*, **570**, 293-305. https://doi.org/10.1016/j.colsurfa.2019.03.036
137. Wang, L., Zhou, H., Zhang, H., Song, Y., Zhang, H., Qian, X., 2020. SiO_2@TiO_2 core@Shell nanoparticles deposited on 2D-layered $ZnIn_2S_4$ to form a ternary heterostructure for simultaneous photocatalytic hydrogen production and organic pollutant degradation. *Inorganic Chemistry*, **59**, 2278-2287. https://doi.org/10.1021/acs.inorgchem.9b03007
138. Zhao, J., Yang, Y., Cui, C., Hu, H., Zhang, Y., Xu, J., Lu, B., Xu, L., Pan, J., Tang, W., 2016. TiO_2 hollow spheres as light scattering centers in TiO_2 photoanodes for dye-sensitized solar cells: The effect of sphere diameter. *Journal of Alloys and Compounds*, **663**, 211-216. https://doi.org/10.1016/j.jallcom.2015.12.118
139. Liu, Y., Wang, S., Shan, Z., Li, X., Tian, J., Mei, Y., Ma, H., Zhu, K., 2012. Electrochimica Acta Anatase TiO_2 hollow spheres with small dimension fabricated via a simple preparation method for dye-sensitized solar cells with an ionic liquid electrolyte. *Electrochim Acta.* **60**, 422–7. https://doi.org/10.1016/j.electacta.2011.11.088
140. Zhao, Y.L., Song, D.M., Qiang, Y.H., Gu, X.Q., Zhu, L., Song, C.B., 2014. Dye-sensitized solar cells based on TiO_2 hollow spheres/TiO_2 nanotube array composite films. *Applied Surface Science*, **309**, 85-9. https://doi.org/10.1016/j.apsusc.2014.04.184
141. Yu, J., Fan, J., Cheng, B., 2011. Dye-sensitized solar cells based on anatase TiO_2 hollow spheres/carbon nanotube composite films. *Journal of Power Sources*, **196**, 7891-8. https://doi.org/10.1016/j.jpowsour.2011.05.014
142. Kanjana, N., Maiaugree, W., Poolcharuansin, P., Laokul, P., 2021. Synthesis and characterization of Fe-doped TiO_2 hollow spheres for dye-sensitized solar cell applications. *Materials Science and Engineering: B*, **271**, 115311. https://doi.org/10.1016/j.mseb.2021.115311
143. Hsu, C.-Y., Al-Salman, H.N.K., Mahmoud, Z.H., Ahmed, R.M., Dawood, A.F., 2024. Improvement of the photoelectric dye sensitized solar cell performance using Fe/S–TiO_2 nanoparticles as photoanode electrode. *Scientific Reports*, **14**. https://doi.org/10.1038/s41598-024-54895-z
144. Song, D.H., Kim, H.-Y., Kim, H.-S., Suh, J.S., Jun, B.-H., Rho, W.-Y., 2017. Preparation of plasmonic monolayer with Ag and Au nanoparticles for dye-sensitized solar cells. *Chemical Physics Letters*, **687**, 152-7. https://doi.org/10.1016/j.cplett.2017.08.051
145. Salimi, K., Atilgan, A., Aydin, M.Y., Yildirim, H., Celebi, N., Yildiz, A., 2019. Plasmonic mesoporous core-shell Ag-Au@TiO_2 photoanodes for efficient light harvesting in dye sensitized solar cells. *Solar Energy*, **193**, 820-827. https://doi.org/10.1016/j.solener.2019.10.039
146. Choi, H., Chen, W.T., Kamat, P.V., 2012. Know thy nano neighbor Plasmonic versus electron charging effects of metal nanoparticles in dye-sensitized solar cells. *ACS Nano*, **6**, 4418-4427. https://doi.org/10.1021/nn301137r
147. Ni, P., De Luna Bugallo, A., Yang, X., Arellano Arreola, V.M., Flores Salazar, M., Strupiechonski, E., Alloing, B., Shan, C., Genevet, P., 2019. Hybrid MoS2-gap-mode metasurface photodetectors. *Journal of Physics D: Applied Physics*, **52**, 374001. https://doi.org/10.1088/1361-6463/ab2aba
148. Lim, S.P., Pandikumar, A., Huang, N.M., Lim, H.N., 2014. Enhanced photovoltaic performance of silver@titania plasmonic photoanode in dye-sensitized solar cells. *RSC Advances*, **4**, 38111-8. https://doi.org/10.1039/c4ra05689b
149. Abadeer, N.S., Brennan, M.R., Wilson, W.L., Murphy, C.J., 2014. Distance and plasmon wavelength dependent fluorescence of molecules bound to silica-coated gold nanorods. *ACS Nano*, **8**, 8392-8406. https://doi.org/10.1021/nn502887j
150. Zhou, G., Zhao, Y., Manthiram, A., 2015. Dual-Confined flexible sulfur cathodes encapsulated in nitrogen-Doped double-Shelled hollow carbon spheres and wrapped with graphene for Li–S batteries. *Advanced Energy Materials*, **5**, 1402263. https://doi.org/10.1002/aenm.201402263
151. Petronella, F., Truppi, A., Dell'Edera, M., Agostiano, A., Curri, M.L., Comparelli, R., 2019. Scalable synthesis of mesoporous TiO_2 for environmental photocatalytic applications. *Materials (Basel, Switzerland)*, **12**, 1853. https://doi.org/10.3390/ma12111853